using an ISOGEN kit (Wako Pure Chemical Industries, Ltd.) was reverse transcribed using Super Script reverse transcriptase (Takara Shuzo Co., Ltd., Shiga, Japan) with random hexamer (Takara Shuzo), and 5% of the reaction mixture was amplified with LA-Taq DNA polymerase (Takara Shuzo) using specific primer pairs: 5′-TGTTGCTGGGAGCTGTTCTACTG-3′ and 5′-ATGTCTCCCTTAGGACCAATAAG-3′ for adiponectin, 5′-GAAGACAGTGGGTA-CATGCGAATG-3′ and 5′-CCTCATGGAGGAA-GGCACTGCTG-3′ for AdipoR1, 5′-GCACCG-CCGAGATGGACTGCTGAA-3′ and 5′-GG-C-GGAAAGAGGATGGAGGTGACG-3′ for AdipoR2, and 5′-CATGTAGGCCATGAGGTCCAC-CAC-3′ and 5′-TGAAGGTCGGTGTGAACGGA-TTTGGC-3′ for G3PDH. Up to 25 cycles of amplification were performed with a Perkin Elmer PCR Thermal Cycler (PE-2400; Perkin-Elmer Corp., Norwalk, CT) at 94°C for 30 sec, at 52–60°C for 60 sec, and at 72°C for 90 sec. As negative controls to exclude genomic amplification, total RNA without reverse transcription was directly used for PCR.

Analysis of Skeletal Morphology

A bone radiograph of whole bodies, femurs, and tibiae was taken with a soft X-ray apparatus (SOFTEX, CMB-2, Tokyo, Japan). Bone mineral density (BMD; mg/cm^2) of the right femurs, tibiae, and L2-L5 vertebral bodies were determined using dual-energy X-ray absorptiometry (DEXA) (PIXImus^{TM} Mouse Densitometer; Lunar Corp., Madison, WI), according to the manufacturer's instructions. All histological analyses were carried out using left tibiae of 8-week-old mice. For the assessment of dynamic histomorphometric indices, mice were injected subcutaneously with 8 mg/kg BW of calcein at 10 days and 3 days before sacrifice. After the sacrifice, the left tibiae were excised, fixed with ethanol, and the undecalcified bones were embedded in glycolmethacrylate. Three micrometers sagittal sections from the proximal parts of the tibiae were stained with Villanueva–Goldner and were visualized under fluorescent light microscopy for calcein labeling. The specimens were subjected to histomorphometric analyses using a semiautomated system (Osteoplan II; Carl Zeiss). Parameters for the trabecular bone were measured in an area 1.2 mm in length from 250 μm below the growth plate at the proximal metaphysis of the tibiae. Nomenclature, symbols, and units are those recommended by the Nomenclature Committee of the American Society for Bone and Mineral Research [Parfitt et al., 1987].

Bone Marrow Cell Cultures

Bone marrow cells were collected from long bones of 8-week-old WT and Ad−/− male littermates. Cells were plated at a density of 10^6 cells on a six-multi-well plate in αMEM containing 10% FBS, with 50 μg/ml ascorbic acid, and 10 mM β-glycerophosphate for osteogenesis assay, and with 1 μM troglitazone for the adipogenesis assay. For the alkaline phosphatase (ALP) staining, cultured plates were rinsed with PBS, fixed in 100% ethanol at 10 days of culture, and stained with Tris-HCl-buffered solution (pH 9.0) containing naphthol AS-MX phosphate as a substrate and Fast Blue BB salt (Sigma-Aldrich, St. Louis, MS) as a coupler. For the Alizarin red staining, cultured plates were rinsed with PBS at 21 days of culture, fixed in 10% buffered formalin, and stained with 2% Alizarin red S (pH 4.0) (Sigma-Aldrich). For the analysis of adipogenesis, the medium was supplemented with 1 μM troglitazone (Sankyo Pharmaceutical Co., Tokyo) for 10 days, fixed in 10 mM sodium periodate, 2% paraformaldehyde, 75 mM L-lysin dihydrochloride, and 37.5 mM sodium phosphate, and then stained in a filtered solution of 0.3% oil red O in 60% isopropanol for 15 min. The red-stained, lipid vacuole-containing cells in a well were counted.

Osteoclast Formation Assay

Tartrate resistant acid phosphatase (TRAP)-positive multi-nucleated osteoclasts were generated by coculturing bone marrow cells (5×10^5 cells/well) and calvarial osteoblasts (1×10^4 cells/well), derived from either WT or Ad−/− littermates, in a 24-multi-well plate for 6 days in αMEM containing 10% FBS and $1,25(OH)_2D_3$ (10 nM). The staining was performed at pH 5.0 in the presence of L(+)-tartaric acid using naphthol AS-MX phosphate (Sigma-Aldrich) in N, *N*-dimethyl formamide as the substrate. Cells positively stained for TRAP containing more than three nuclei were counted as osteoclasts.

Effects of Recombinant Adiponectin on Bone Marrow Cells and ST2 Cells

Recombinant mouse full-length adiponectin expressed in *Escherichia coli* was isolated and

purified as previously described [Yamauchi et al., 2003a]. Bone marrow cells collected from long bones of WT mice were plated at a density of 10^6 cells/well in a six-multi-well plate, cultured with 0, 3, and 10 μg/ml of recombinant adiponectin in αMEM/10% FBS/ascorbic acid/β-glycerophosphate in the presence and absence of insulin (10 nM), and stained with ALP and Alizarin red after 10 and 21 days, respectively, as described above. ST2 cells were inoculated at a density of 1×10^4 cells/well in a 24-multi-well plate, cultured with 0, 1, 3 and 10 μg/ml of recombinant adiponectin in αMEM/10% FBS/ascorbic acid with insulin-like growth factor-I (IGF-I, 100 nM) or bone morphogenetic protein-2 (BMP-2, 10 nM). At 7 days of culture, cells were sonicated in 10 mM Tris-HCl buffer (pH 8.0) containing 1 mM $MgCl_2$ and 0.5% Triton X-100. ALP activity in the lysate was measured using a Wako ALP kit (Wako Pure Chemical) and the protein content was determined using BCA protein assay reagent (Pierce Biotechnology, Rockford, IL).

Immunoprecipitation and Immunoblotting

For immunoprecipitation and immunoblotting, bone marrow cells collected from long bones of WT mice were plated at a density of 2×10^6 cells/well in a 6 cm dish and cultured for 10 days as described above. After 6 h of serum starvation, cells were cultured with or without 10 μg/ml of recombinant adiponectin for 24 h. Cells were then stimulated with insulin (100 nM) or the vehicle for 10 min, and lysed with TNE buffer (10 mM Tris-HCl, 150 mM NaCl, 1% NP-40, 1 mM EDTA, 10 mM NaF, 2 mM Na_3VO_4, 1 mM aminoethyl-benzenesulfonyl fluoride, and aprotinin). A part of the cell lysates (100 μg) were immunoprecipitated with an anti-insulin receptor substrate (IRS)-1 antibody (Upstate, Waltham, MA) conjugated to protein G-Sepharose (Invitrogen) overnight at 4°C. The cell lysates with or without the immunoprecipitation that contained an equivalent amount of protein (20 μg) were electrophoresed by 8% SDS–PAGE, and transferred to PVDF membrane. After blocking with 5% BSA solution, they were incubated with either anti-phosphotyrosine (clone 4G10), anti-mouse phospho-Akt (Ser 472), anti-mouse Akt, or anti-mouse IRS-1 antibody (all from Upstate). Immunoreactive bands were stained using the ECL chemiluminescence reaction (Amersham Co., Arlington Heights, IL).

Statistical Analysis

Means of groups were compared by ANOVA and significance of differences was determined by post hoc testing using Bonferroni's method.

RESULTS

Expressions of Adiponectin and its Receptors in Bone Cells

Because adiponectin and its two receptors AdipoR1 and AdipoR2 were reported to be differentially expressed in a variety of cells and tissues [Yamauchi et al., 2003a; Berner et al., 2004], we first investigated their expressions in cells of osteoblastic and osteoclastic lineages by RT-PCR (Fig. 1). All mRNA expressions were detected in bone marrow cells, calvarial osteoblasts, osteoclast precursor M-BMMΦ, and isolated mature osteoclasts that were derived from WT mice, suggesting that they are ubiquitously expressed in various

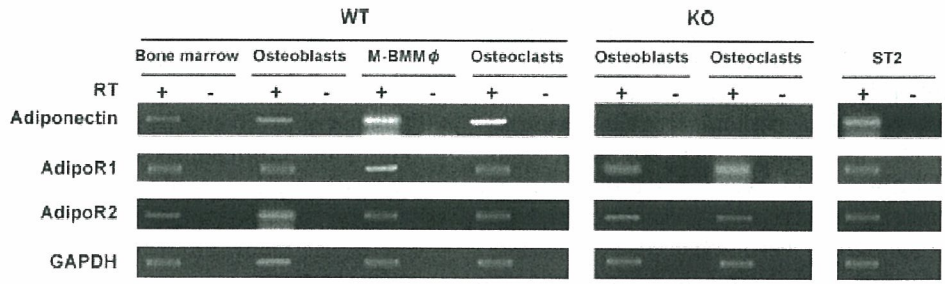

Fig. 1. Expressions of adiponectin and its receptors AdipoR1 and AdipoR2 in cells of osteoblastic and osteoclastic lineages derived from WT and Ad−/− mice by RT-PCR. Total RNA was extracted from bone marrow cells collected from adult mouse long bones, neonatal mouse calvarial osteoblasts, osteoclast precursor M-CSF-dependent bone marrow macrophages (M-BMMΦ), mature osteocalsts formed and isolated from the culture of M-BMMΦ with M-CSF and RANKL, and mouse bone marrow-derived stromal cell line ST2 cells. An aliquot of total RNA with (+) or without (−) reverse transcription (RT) was amplified using specific primers within an exponential phase of the amplification.

kinds of cells in bone. Although adiponectin was confirmed not to be expressed in the Ad−/− cells, AdipoR1, and AdipoR2 were detected in both osteoblasts and osteoclasts. In addition, all were also detected in a mouse stromal cell line ST2. These results indicate that adiponectin acts on bone not only through an endocrine pathway as a hormone secreted from fat tissue, but also through an autocrine/paracrine pathway. To elucidate the actions of adiponectin through these distinct pathways, we next performed experiments using the deficient and overexpressing transgenic mice.

No Abnormality in Bone of Adiponectin-Deficient Mice In Vivo

To examine the role of endogenous adiponectin in bone metabolism, we analyzed the bones of Ad−/− mice. Ad−/− mice developed and grew normally, indicating that adiponectin is not involved in the regulation of skeletal growth. X-ray analyses showed no significant difference in the skeleton between Ad−/− and WT littermates at 8 weeks of age (Fig. 2A). BMDs of the entire femurs, tibiae, and vertebrae (L2-L5) were also similar between mice of the two genotypes (Fig. 2B). In accordance with X-ray and BMD findings, histological analyses of the proximal tibiae of 8-week-old Ad−/− mice by the Villanueva–Goldner staining revealed no difference in bone phenotypes from those of WT littermates (Fig. 2C). The growth plate at the proximal tibiae of Ad−/− mice also seemed similar to that of WT, consistent with the lack of contribution of adiponectin to the skeletal growth. Bone histomorphometric measurements in this area supported these histological observations (Table I): there was no difference between Ad−/− and WT littermates in bone volume (BV/TV), bone formation parameters (Ob.S/BS & BFR), or bone resorption parameters (Oc.S/BS & ES/BS).

Suppression of Osteogenesis in the Culture of Adiponectin-Deficient Bone Marrow Cells

Considering that adiponectin acts through both endocrine and autocrine/paracrine pathways, the lack of abnormal phenotype in the bones of Ad−/− mice, which are not bone-specific conditional knockout mice but conventional knockout mice, may possibly be due to the equivalent balance of the two pathways. To examine the specific effect of the autocrine/paracrine action of adiponectin, in vitro cultures of bone marrow cells from Ad−/− and WT mice were compared. Surprisingly, osteogenesis determined by the number of colonies positively stained with ALP and Alizarin red was significantly decreased in the Ad−/− marrow cell culture as compared with that in the WT culture, suggesting a positive effect of the autocrine/paracrine action on bone formation (Fig. 3A, left and middle panels). However,

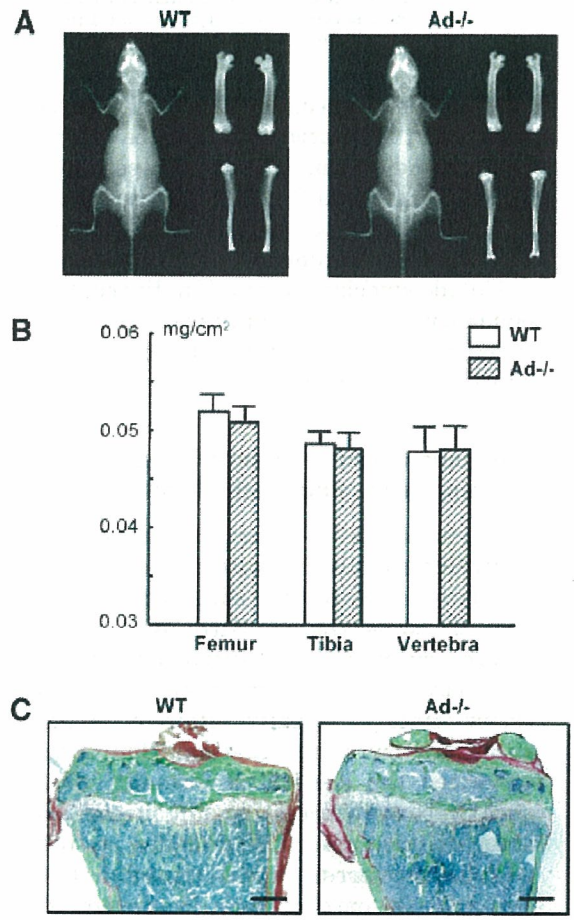

Fig. 2. Radiological and histological findings of the bones in male WT and Ad−/− littermates (8 weeks old). **A**: Plain X-ray images of the whole bodies (**left**), femurs (**upper right**), and tibiae (**lower right**) of representative WT and Ad−/− littermates. **B**: BMD of the entire femurs, tibiae, and L2-L5 vertebral bodies determined by DEXA. Data are expressed as means (bars) ± SEM (error bars) of 10 bones/group. None of the bones showed significant difference of BMD between the two genotypes. **C**: Histological features of the proximal tibiae of representative mice of each genotype. After the sacrifice, the tibiae were excised, fixed, embedded without decalcification, and the sagittal sections were stained with Villanueva–Goldner, in which mineralized bone was stained green and unmineralized osteoid red. Bar, 100 μm. Data of histomorphometric analyses are shown in Table I. [Color figure can be viewed in the online issue, which is available at www.interscience.wiley.com.]

TABLE I. Histomorphometry of Trabecular Bones in Proximal Tibiae of WT and Ad−/−Mice

	BV/TV (%)	Ob.S/BS (%)	BFR (mm^3/cm^2/year)	Oc.S/BS (%)	ES/BS (%)
WT	12.75 ± 0.96	11.93 ± 0.90	3.66 ± 0.92	4.58 ± 1.78	3.52 ± 0.79
Ad−/−	10.71 ± 1.92	12.07 ± 1.22	3.16 ± 0.93	4.32 ± 1.38	3.82 ± 0.89

Parameters for the trabecular bone were measured in an area 1.2 mm in length from 250 μm below the growth plate at the proximal metaphysis of the tibiae in Villanueva–Goldner and calcein double-labeled sections. Data expressed as means and standard errors (SEM) for 10 bones/group.
No significant difference of parameters between two genotypes (all $P > 0.05$).
BV/TV, trabecular bone volume expressed as a percentage of total tissue volume; Ob.S/BS, percentage of bone surface covered by cuboidal osteoblasts; BFR, bone formation rate; Oc.S/BS, percentage of bone surface covered by mature osteoclasts; ES/BS, percentage of eroded surface.

adipogenesis determined by the oil red O staining in the marrow cell culture was similar between Ad−/− and WT marrow cell cultures (Fig. 3A; right panel). To investigate the role of local adiponectin in osteoclastic cells, we next measured the number of TRAP-positive multinucleated osteoclasts formed in the coculture of bone marrow cells and primary osteoblasts, and found no difference between the cells of the two genotypes (Fig. 3B).

No Abnormality in Bone of Transgenic Mice Overexpressing Adiponectin in the Liver In Vivo

The in vivo Ad−/− bone analyses showed the equivalent balance of autocrine/paracrine and endocrine actions of adiponectin on bone (Fig. 2), while the in vitro Ad−/− marrow culture revealed the positive autocrine/paracrine action on bone formation (Fig. 3). These results imply a negative effect of circulating adiponectin on bone formation. Hence, we next examined the skeletal abnormality of transgenic mice overexpressing adiponectin (Ad-Tg) being driven by the SAP promoter, so that the adiponectin expression was limited to the liver and was not in the bone [Yamauchi et al., 2003b]. Ad-Tg mice appeared normal and indistinguishable from WT littermates in body weight and length. Plain X-ray images of Ad-Tg mice at 8 weeks showed no abnormality in the skeleton compared with WT littermates (Fig. 4A), and BMDs of the entire femurs, tibiae, and vertebrae (L2-L5) of Ad-Tg mice were also similar to those of WT littermates (Fig. 4B). Histological analyses of the proximal tibiae by the Villanueva–Goldner staining (Fig. 4C) and bone histomorphometric measurements (Table II) confirmed that neither the bone mass nor the bone turnover was affected by the circulating adiponectin.

Suppression of Osteogenesis by Recombinant Adiponectin in Osteoprogenitor Cell Cultures

We failed to detect the expected negative effect of circulating adiponectin on bone formation in Ad-Tg mice in vivo. However, since adiponectin is known to enhance the insulin action on its target organs [Berg et al., 2001; Combs et al., 2001; Fruebis et al., 2001; Yamauchi et al., 2001, 2003b; Kubota et al., 2002], the effect of circulating adiponectin on bone might partly be mediated by the insulin signaling that is anabolic for bone formation [Thomas et al., 1996]. Hence, we next looked at the systemic (or endocrine) action by examining the effect of addition of recombinant adiponectin on osteogenesis in cultures of osteoprogenitor cells in the presence and absence of insulin. In the cultures of bone marrow cells derived from WT long bones, osteogenesis determined by the numbers of colonies positively stained with ALP and Alizarin red were dose-dependently inhibited by recombinant adiponectin in the absence of insulin, indicating a direct/negative action of adiponectin on bone formation (Fig. 5A). However, in the presence of insulin (10 nM), the inhibition of osteogenesis by adiponectin was not seen in either ALP or Alizarin red staining. In the culture of mouse stromal cell line ST2, recombinant adiponectin also did not decrease ALP activity which was stimulated by IGF-I (100 nM), another bone anabolic factor that shares downstream molecules with the insulin signaling (Fig. 5B). In contrast, it dose-dependently decreased ALP activity which was stimulated by BMP-2 (10 nM).

We then investigated the effect of adiponectin on the intracellular signaling of insulin in bone marrow cells by examining the phosphorylations

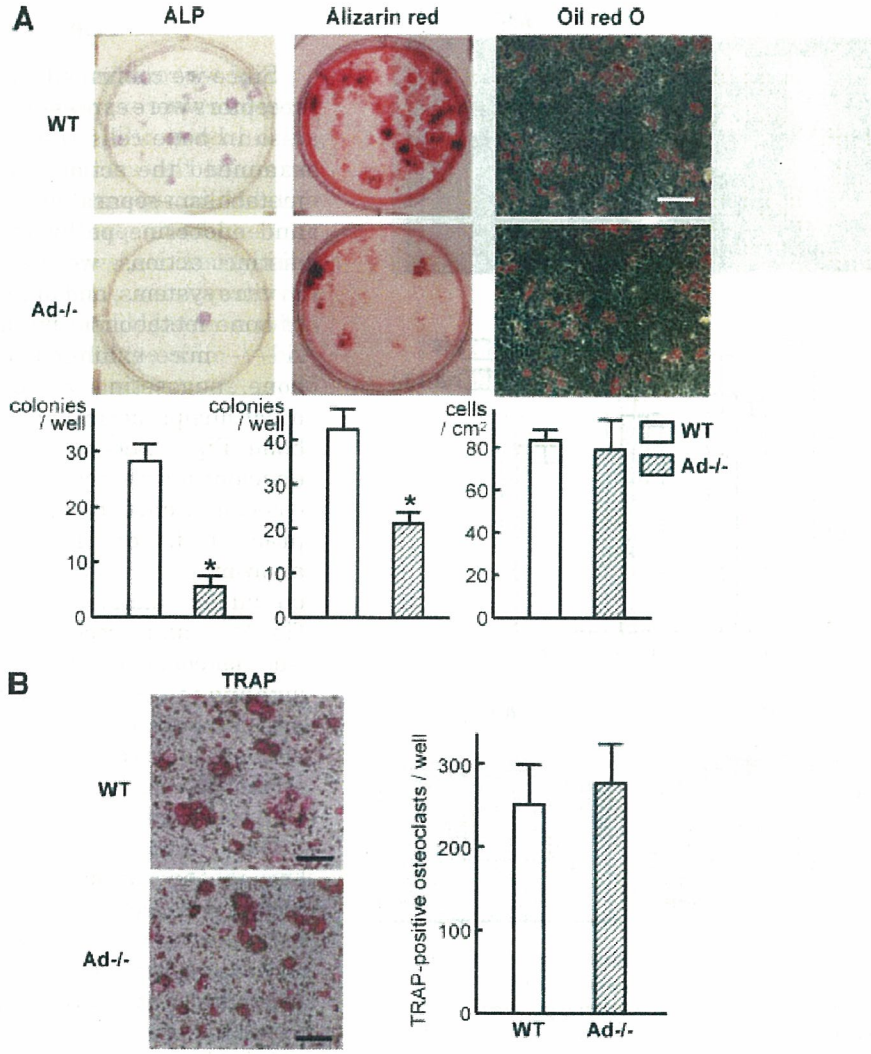

Fig. 3. Osteogenesis, adipogenesis, and osteoclastogenesis in cultures of bone marrow cells from WT and Ad−/− littermates. **A**: Osteogenesis was determined by ALP (**left**) and Alizarin red (**middle**) stainings of bone marrow cells cultured for 10 and 21 days, respectively, in αMEM/10% FBS with ascorbic acid and β-glycerophosphate. Adipogenesis was determined by oil red O staining (**right**) of bone marrow cells cultured for 10 days in αMEM/10% FBS with troglitazone. Bar, 200 μm. The graphs below indicate the number of positive colonies/well for ALP and Alizarin red stainings, and of positive cells/cm^2 for oil red O staining. Data are expressed as means (bars) ± SEMs (error bars) for eight wells/group. *, significant difference from the WT culture; $P < 0.01$. **B**: Osteoclastogensis was determined by the number of TRAP-positive multi-nucleated osteoclasts formed in the coculture of bone marrow cells and calvarial osteoblasts from WT and Ad−/− littermates in αMEM/10% FBS with 1,25$(OH)_2D_3$ for 6 days. Bar, 400 μm. Data are expressed as mean (bars) ± SEM (error bars) for eight wells/group. There was no significant difference between WT and Ad−/− cultures. [Color figure can be viewed in the online issue, which is available at www.interscience.wiley.com.]

of IRS-1 and Akt, the main downstream molecules of insulin. Immunoprecipitation and immunoblotting analyses revealed that phosphorylations of IRS-1 and Akt were induced by insulin alone, while hardly being affected by recombinant adiponectin alone. More importantly, the phosphorylations induced by insulin were further enhanced by adiponectin, suggesting indirect/positive action of adiponectin on bone formation via enhancement of the insulin signaling (Fig. 5C).

The results indicate that no bone abnormality in Ad-Tg mice may be possibly due to an equivalent balance of the direct/negative and indirect/positive actions of circulating adiponectin. The direct action might possibly be related to the BMP signaling, and the indirect one may be through enhancement of the insulin signaling.

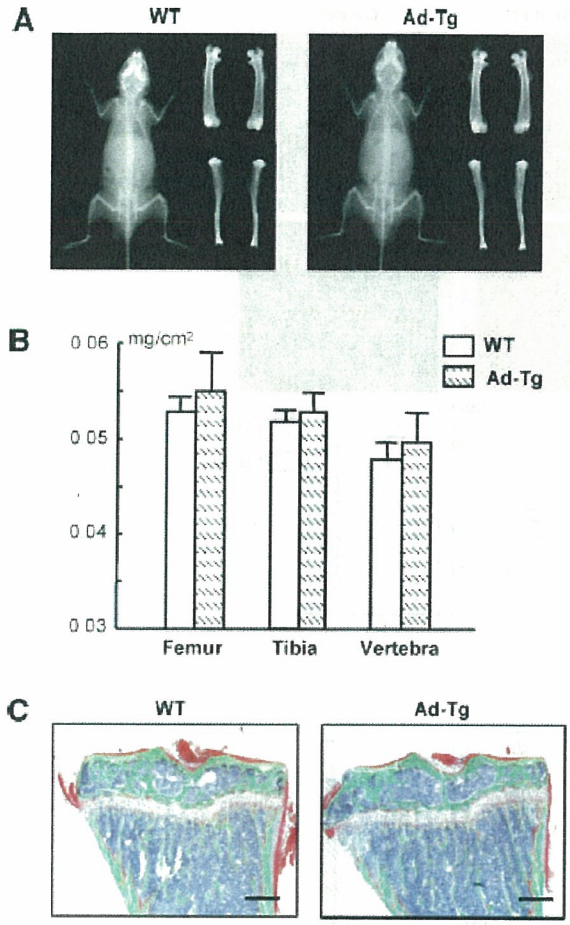

Fig. 4. Radiological and histological findings of the bones in male WT and Ad-Tg littermates (8 weeks old). **A**: Plain X-ray images of the whole bodies (**left**), femurs (**upper right**), and tibiae (**lower right**) of representative WT and Ad-Tg littermates. **B**: BMD of the entire femurs, tibiae, and L2-L5 vertebral bodies determined by DEXA. Data are expressed as means (bars) ± SEM (error bars) of 10 bones/group. None of the bones showed significant difference of BMD between the two genotypes. **C**: Histological features of the proximal tibiae of representative mice of the two genotypes prepared as described in Figure 2. Bar, 100 μm. Data of histomorphometric analyses are shown in Table II. [Color figure can be viewed in the online issue, which is available at www.interscience.wiley.com.]

DISCUSSION

Since we confirmed that adiponectin and its receptors were expressed not only in fat cells but also in bone cells (Fig. 1), the present study examined the actions of adiponectin on bone metabolism separately via autocrine/paracrine and endocrine pathways. To elucidate these distinct actions, we used several in vivo and in vitro systems, and found variable regulations of bone metabolism by adiponectin. First, the Ad−/− mice exhibited no abnormality in the bone, suggesting an equivalent balance of autocrine/paracrine and endocrine actions on bone (Fig. 2). Second, the in vitro adiponectin-deficient marrow cell culture revealed a potent osteogenic effect of adiponectin as an autocrine/paracrine factor (Fig. 3). Third, the lack of bone abnormality in the Ad-Tg mice indicated an equivalent balance of circulating adiponectin (Fig. 4). Lastly, recombinant adiponectin inhibited osteogenesis but enhanced the insulin signaling in osteoprogenitor cell cultures, suggesting the direct/negative and indirect/positive actions of circulating adiponectin on bone formation (Fig. 5). It is therefore speculated that there are at least three distinct adiponectin actions on bone formation: a positive action through the autocrine/paracrine pathway by locally produced adiponectin in bone, a negative action through the direct pathway by circulating adiponectin, and a positive action through the indirect pathway by circulating adiponectin via enhancement of the insulin signaling.

It is of note that effects of adiponectin on bone formation differed among experimental systems, that is, between in vivo and in vitro; between gain-of-function and loss-of-function. These discrepancies are also seen in the actions of leptin, another representative adipokine.

TABLE II. Histomorphometry of Trabecular Bones in Proximal Tibiae of WT and Ad-Tg Mice

	BV/TV (%)	Ob.S/BS (%)	BFR (mm^3/cm^2/year)	Oc.S/BS (%)	ES/BS (%)
WT	11.38 ± 0.67	10.38 ± 0.83	4.96 ± 0.62	5.49 ± 1.39	5.02 ± 0.90
Ad-Tg	13.97 ± 0.62	13.70 ± 1.01	5.06 ± 0.29	6.93 ± 1.87	4.42 ± 1.95

Parameters for the trabecular bone were measured in an area 1.2 mm in length from 250 mm below the growth plate at the proximal metaphysis of the tibiae in Villanueva–Goldner and calcein double-labeled sections. Data expressed as means and standard errors (SEM) for 10 bones/group.
No significant difference of parameters between two genotypes (all $P > 0.05$).
BV/TV, trabecular bone volume expressed as a percentage of total tissue volume; Ob.S/BS, percentage of bone surface covered by cuboidal osteoblasts; BFR, bone formation rate; Oc.S/BS, percentage of bone surface covered by mature osteoclasts; ES/BS, percentage of eroded surface.

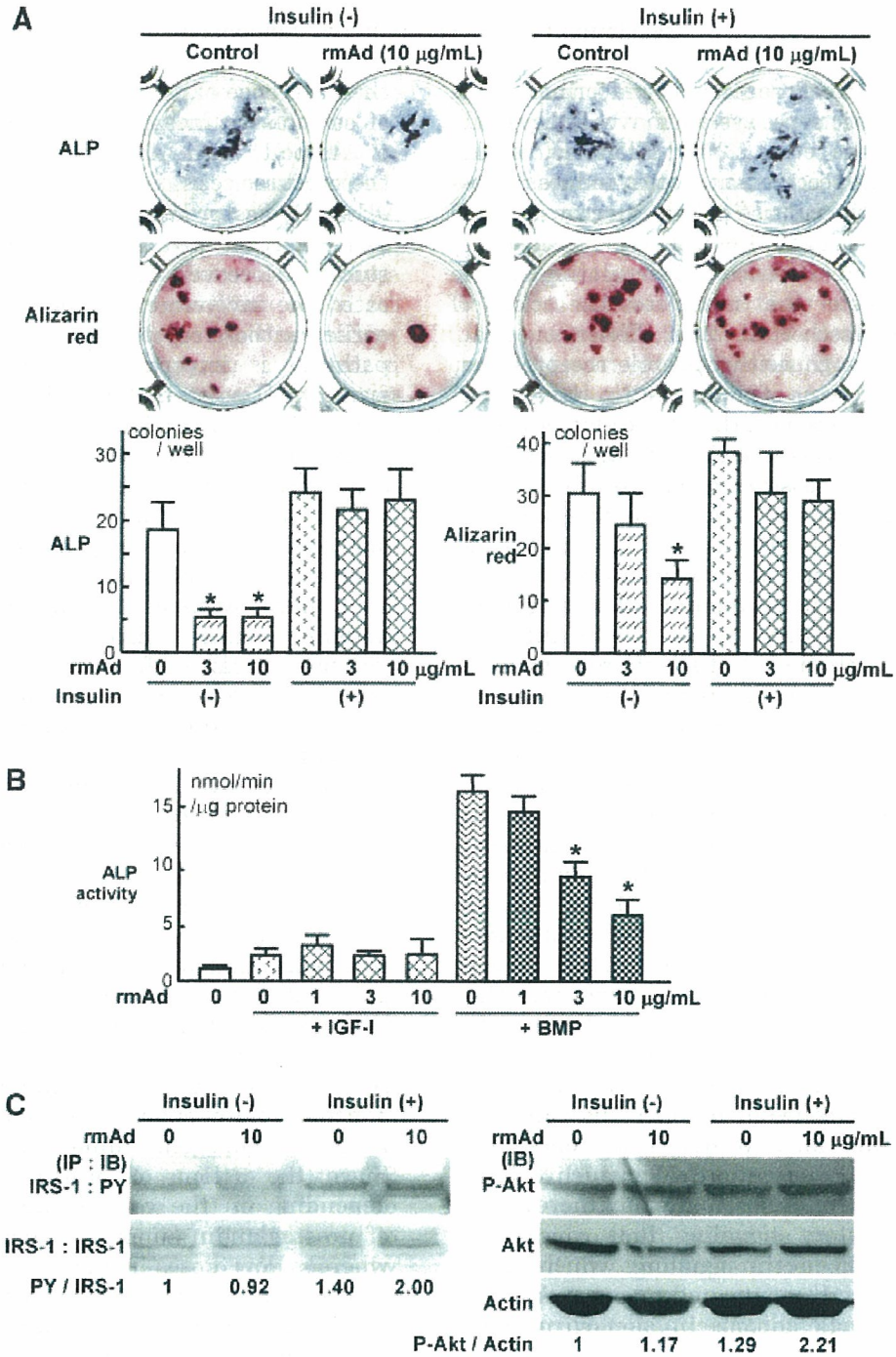

Fig. 5. **A**: Effect of recombinant mouse adiponectin (rmAd) on osteogenesis in the bone marrow cell culture. Osteogenesis was determined by ALP and Alizarin red stainings after 10 and 21 days of culture, respectively, with indicated concentrations of rmAd in αMEM/10% FBS/ascorbic acid/β-glycerophosphate with or without insulin (10 nM). The graphs below indicate the number of positive colonies/well. Data are expressed as means (bars) ± SEMs (error bars) for eight wells/group. *, significant inhibition by rmAd; $P < 0.01$. **B**: Effect of rmAd on ALP activity of ST2 cells cultured for 7 days with indicated concentrations of rmAd in αMEM/10% FBS/ascorbic acid and IGF-1 (100 nM) or BMP-2 (10 nM). Data are expressed as means (bars) ± SEMs (error bars) for eight wells/group. *, significant inhibition by rmAd; $P < 0.01$. **C**: Effect of rmAd on phosphorylations of IRS-1 and Akt in cultured bone marrow cells. Protein levels of phosphorylated IRS-1, IRS-1, phosphorylated Akt, Akt, and β-actin were determined by immunoprecipitation (IP) and immunoblotting (IB) in the cells stimulated by insulin (100 nM) or the vehicle for 10 min after pre-treatment with or without rmAd (10 μg/ml) for 24 h. The number under each band shows the ratio of the band intensity of phosphorylated IRS-1 and phosphorylated Akt normalized to those of IRS-1 and β-actin, respectively, that were measured by densitometry. Similar results were obtained in five independent experiments. [Color figure can be viewed in the online issue, which is available at www.interscience.wiley.com.]

Leptin negatively regulates bone formation via a sympathetic nerve system in vivo [Ducy et al., 2000; Takeda et al., 2002; Elefteriou et al., 2004], while recombinant leptin induces osteogenesis in the culture of bone marrow stromal cells [Thomas et al., 1999]. This is implicated to be due to the existence of a circulating soluble leptin receptor that modulates the action of leptin [Kratzsch et al., 2002; Elefteriou et al., 2004]. Although neither soluble receptors nor binding proteins of adiponectin have been identified, it is possible that the co-factors might explain the diverse actions of adiponectin on bone. Another possible mechanism underlying the discrepancy may be a variety of adiponectin forms, since it is present as a full length or as cleavage products such as an active form C-terminal globular fragment in plasma [Fruebis et al., 2001; Kishida et al., 2003]. Although biological activities of the different forms of adiponectin are poorly understood, they might be specific for distinct receptors and cell types. Recently, Oshima et al. [2005] reported that a single injection of adenovirus expressing a full-length adiponectin increased bone mass by stimulating bone formation and suppressing bone resorption. In contrast, the present bone histomorphometric analysis of Ad-Tg mice with constitutive overexpression of the globular form of adiponectin revealed no abnormality in bone formation or bone resorption parameter. This difference may not be due to that of the molecular form since our preliminary investigation of the transgenic mice that overexpress the full-length adiponectin driven by the same SAP promoter also failed to show bone abnormality (unpublished observation by Yamauchi & Kadowaki). We therefore speculate that there may be a compensatory signaling that cancels the excessive adiponectin signaling, which cannot catch up with the acute and strong overexpression by a single adiponectin-adenovirus application.

The present in vitro experiments showed that recombinant full-length adiponectin at the physiological serum concentration (10 μg/ml) [Kubota et al., 2002] inhibited osteogenic differentiation from bone marrow cells and mouse stromal cell line ST2, which is also inconsistent with previous studies showing that it increased the differentiation and mineralization in the murine osteoblast cell line MC3T3-E1 cell and human primary osteoblast cultures [Luo et al., 2005; Oshima et al., 2005]. This might be due to the difference of differentiation stages of cells of osteoblastic lineage. The expression levels of AdipoR1 and AdipoR2 were similar in the precursor cells of the present study, while AdipoR1 was predominantly expressed in the more differentiated osteoblasts of the previous studies. Moreover, although this study implicated the involvement of the BMP pathway, earlier authors reported that the MAP kinase pathway is important for the adiponectin signaling [Luo et al., 2005]. In fact, our study using a mouse calvarial osteoblast culture failed to show the inhibitory effect of the recombinant adiponectin (data not shown). Another explanation for the discrepancy between the present and previous results may be the existence of other lineage of cells than osteoprogenitors in our culture systems, but not in the earlier systems. Because adiponectin is reported to variably regulate differentiation of bone marrow cells into several lineages through the ubiquitously expressed receptors, it is possible that adiponectin can affect other lineage of cells like lymphocytes and adipocytes, causing a proportional decrease of osteoprogenitors in bone marrow. It is known to inhibit B lymphopoiesis through induction of prostaglandin synthesis, but stimulates myelopoiesis [Yokota et al., 2003]. It also suppresses adipogenesis from bone marrow cells through a cyclooxygenase-2/prostaglandin-dependent mechanism [Yokota et al., 2002]; however, the present study showed normal adipogenesis from cultured Ad−/− marrow cells, suggesting the difference of actions of exogenous and endogenous adiponectin on adipogenic differentiation as well. Since the actions of prostaglandins differ depending on the concentration; high doses of prostaglandin suppress collagen synthesis whereas low doses induce it in osteoblasts [Chyun and Raisz, 1984], the actions of adiponectin on bone might be mediated in part by prostaglandin production, so that they differ depending on the concentration. Insofar as the effects of adiponectin on these other types of cells remain unclarified, we should acknowledge that the present study does not reach a definitive conclusion relating to the mechanism of adiponectin on bone homeostasis.

In addition to the direct and negative effect on the osteoprogenitor cells, circulating adiponectin exhibited a positive effect on bone formation through enhancement of the insulin signaling. There is a great deal of evidence supporting that

adiponectin increases the insulin action in its target organs. Recombinant adiponectin ameliorated insulin resistance in obese- and diabetic-KKA^y mice and diabetic-lipoatrophic mice, both of which had reduced plasma adiponectin levels [Yamauchi et al., 2001]. A single injection of recombinant adiponectin abolished hyperglycemia by suppressing glucose production in ob/ob, non-obese diabetic, or streptozotocin-treated mice [Berg et al., 2001; Combs et al., 2001]. Transgenic overexpression of adiponectin also ameliorated insulin resistance in ob/ob mice [Yamauchi et al., 2003b] and the disruption of the adiponectin gene is known to cause insulin resistance [Matsuzawa et al., 2004; Luo et al., 2005]. Another plausible hormone that might be related to the endocrine action of adiponectin might be estrogen, which is also a potent regulator of bone metabolism [Tanko and Christiansen, 2004]. A recent report demonstrated that estrogen can suppress adiponectin secretion in mice and cultured adipocytes [Combs et al., 2003], although the interactions of signalings among adiponectin, estradiol, and insulin in bone are complicated and remain to be further clarified [Kalish et al., 2003].

Regarding the clinical evidence of involvement of adiponectin in bone metabolism, Kontogianni et al. [2004] reported that the circulating level of adiponectin was not correlated with bone mass of perimenopausal women while that of leptin showed an inverse correlation. This is in accordance with the present results that both deficient and overexpressing transgenic mice of adiponectin showed normal bone mass. However, another clinical study by Lenchik et al. [2003] reported significant inverse correlations of adiponectin with visceral fat and BMD, and proposed adiponectin as a mediator of the protective effects of visceral fat mass on BMD. The correlations may be dependent on the balance of the direct and indirect actions of circulating adiponectin, which we showed oppositely affected bone metabolism. When we compare the populations of the two clinical studies above, more subjects (86%) in the study by Lenchik et al. were affected by type 2 diabetes than those in the study by Kontogianni et al. This might at least partly explain the discrepancy of the two clinical studies: in the former the indirect and positive effect of circulating adiponectin was suppressed due to the impaired insulin signaling, so that the direct and negative effect became predominant, while in the latter study there remained an equivalent balance between direct and indirect effects.

Adiponectin is structurally similar to TNF-α, receptor activator of nuclear factor κB ligand (RANKL) and osteoprotegerin, all of which are potent regulators of osteoclastogenesis [Ouchi et al., 2000; Tsao et al., 2002]. However, osteoclastogenesis from marrow cells was not affected by the deficiency of endogenous adiponectin (Ad−/−) in the present study, while a previous study showed a decrease of osteoclastogenesis by adiponectin in vivo and in vitro [Oshima et al., 2005]. This also indicates that there might be distinct effects of adiponectin on osteoclastogenesis through autocrine/paracrine and endocrine pathways. Considering that adiponectin expression is regulated by several bone regulators: it is reduced by TNF-α [Yokota et al., 2000], IL-6 [Kappes and Loffler, 2000], β-adrenergic agonists [Fasshauer et al., 2003], and glucocorticoids [Halleux et al., 2001], whereas stimulated by proliferator-activated receptor (PPARγ) agonists [Combs et al., 2002], adiponectin may play a role in the complicated molecular network that regulates bone metabolism.

ACKNOWLEDGMENTS

We thank Reiko Yamaguchi for providing expert technical assistance. Regrettably, Masayuki Yamaguchi died much young and before the publication of this study. We dedicate this study to him and his family. This work was supported by Grant-in-Aid for Scientific Research from the Japanese Ministry of Education, Culture, Sports, Science, and Technology Grant no. 17591551.

REFERENCES

Arita Y, Kihara S, Ouchi N, Takahashi M, Maeda K, Miyagawa J, Hotta K, Shimomura I, Nakamura T, Miyaoka K, Kuriyama H, Nishida M, Yamashita S, Okubo K, Matsubara K, Muraguchi M, Ohmoto Y, Funahashi T, Matsuzawa Y. 1999. Paradoxical decrease of an adipose-specific protein, adiponectin, in obesity. Biochem Biophys Res Commun 257:79–83.

Berg AH, Combs TP, Du X, Brownlee M, Scherer PE. 2001. The adipocyte-secreted protein Acrp30 enhances hepatic insulin action. Nat Med 7:947–953.

Berner HS, Lyngstadaas SP, Spahr A, Monjo M, Thommesen L, Drevon CA, Syversen U, Reseland JE. 2004. Adiponectin and its receptors are expressed in bone-forming cells. Bone 35:842–849.

Chyun YS, Raisz LG. 1984. Stimulation of bone formation by prostaglandin E2. Prostaglandins 27:97–103.

Combs TP, Berg AH, Obici S, Scherer PE, Rossetti L. 2001. Endogenous glucose production is inhibited by the adipose-derived protein Acrp30. J Clin Invest 108: 1875–1881.

Combs TP, Wagner JA, Berger J, Doebber T, Wang WJ, Zhang BB, Tanen M, Berg AH, O'Rahilly S, Savage DB, Chatterjee K, Weiss S, Larson PJ, Gottesdiener KM, Gertz BJ, Charron MJ, Scherer PE, Moller DE. 2002. Induction of adipocyte complement-related protein of 30 kilodaltons by PPARgamma agonists: A potential mechanism of insulin sensitization. Endocrinology 143: 998–1007.

Combs TP, Berg AH, Rajala MW, Klebanov S, Iyengar P, Jimenez-Chillaron JC, Patti ME, Klein SL, Weinstein RS, Scherer PE. 2003. Sexual differentiation, pregnancy, calorie restriction, and aging affect the adipocyte-specific secretory protein adiponectin. Diabetes 52:268–276.

Diez JJ, Iglesias P. 2003. The role of the novel adipocyte-derived hormone adiponectin in human disease. Eur J Endocrinol 148:293–300.

Ducy P, Amling M, Takeda S, Priemel M, Schilling AF, Beil FT, Shen J, Vinson C, Rueger JM, Karsenty G. 2000. Leptin inhibits bone formation through a hypothalamic relay: A central control of bone mass. Cell 100:197–207.

Elefteriou F, Takeda S, Ebihara K, Magre J, Patano N, Kim CA, Ogawa Y, Liu X, Ware SM, Craigen WJ, Robert JJ, Vinson C, Nakao K, Capeau J, Karsenty G. 2004. Serum leptin level is a regulator of bone mass. Proc Natl Acad Sci USA 101:3258–3263.

Fasshauer M, Kralisch S, Klier M, Lossner U, Bluher M, Klein J, Paschke R. 2003. Adiponectin gene expression and secretion is inhibited by interleukin-6 in 3T3-L1 adipocytes. Biochem Biophys Res Commun 301:1045–1050.

Felson DT, Zhang Y, Hannan MT, Anderson JJ. 1993. Effects of weight and body mass index on bone mineral density in men and women: The Framingham study. J Bone Miner Res 8:567–573.

Fruebis J, Tsao TS, Javorschi S, Ebbets-Reed D, Erickson MR, Yen FT, Bihain BE, Lodish HF. 2001. Proteolytic cleavage product of 30-kDa adipocyte complement-related protein increases fatty acid oxidation in muscle and causes weight loss in mice. Proc Natl Acad Sci USA 98:2005–2010.

Halleux CM, Takahashi M, Delporte ML, Detry R, Funahashi T, Matsuzawa Y, Brichard SM. 2001. Secretion of adiponectin and regulation of apM1 gene expression in human visceral adipose tissue. Biochem Biophys Res Commun 288:1102–1107.

Hotta K, Funahashi T, Arita Y, Takahashi M, Matsuda M, Okamoto Y, Iwahashi H, Kuriyama H, Ouchi N, Maeda K, Nishida M, Kihara S, Sakai N, Nakajima T, Hasegawa K, Muraguchi M, Ohmoto Y, Nakamura T, Yamashita S, Hanafusa T, Matsuzawa Y. 2000. Plasma concentrations of a novel, adipose-specific protein, adiponectin, in type 2 diabetic patients. Arterioscler Thromb Vasc Biol 20: 1595–1599.

Hu E, Liang P, Spiegelman BM. 1996. AdipoQ is a novel adipose-specific gene dysregulated in obesity. J Biol Chem 271:10697–10703.

Kalish GM, Barrett-Connor E, Laughlin GA, Gulanski BI. 2003. Association of endogenous sex hormones and insulin resistance among postmenopausal women: Results from the postmenopausal estrogen/progestin intervention trial. J Clin Endocrinol Metab 88:1646–1652.

Kappes A, Loffler G. 2000. Influences of ionomycin, dibutyryl-cycloAMP and tumour necrosis factor-alpha on intracellular amount and secretion of apM1 in differentiating primary human preadipocytes. Horm Metab Res 32:548–554.

Kharroubi I, Rasschaert J, Eizirik DL, Cnop M. 2003. Expression of adiponectin receptors in pancreatic beta cells. Biochem Biophys Res Commun 312:1118–1122.

Kishida K, Nagaretani H, Kondo H, Kobayashi H, Tanaka S, Maeda N, Nagasawa A, Hibuse T, Ohashi K, Kumada M, Nishizawa H, Okamoto Y, Ouchi N, Maeda K, Kihara S, Funahashi T, Matsuzawa Y. 2003. Disturbed secretion of mutant adiponectin associated with the metabolic syndrome. Biochem Biophys Res Commun 306:286–292.

Kobayashi K, Takahashi N, Jimi E, Udagawa N, Takami M, Kotake S, Nakagawa N, Kinosaki M, Yamaguchi K, Shima N, Yasuda H, Morinaga T, Higashio K, Martin TJ, Suda T. 2000. Tumor necrosis factor alpha stimulates osteoclast differentiation by a mechanism independent of the ODF/RANKL-RANK interaction. J Exp Med 191: 275–286.

Kontogianni MD, Dafni UG, Routsias JG, Skopouli FN. 2004. Blood leptin and adiponectin as possible mediators of the relation between fat mass and BMD in perimenopausal women. J Bone Miner Res 19:546–551.

Kratzsch J, Lammert A, Bottner A, Seidel B, Mueller G, Thiery J, Hebebrand J, Kiess W. 2002. Circulating soluble leptin receptor and free leptin index during childhood, puberty, and adolescence. J Clin Endocrinol Metab 87:4587–4594.

Kubota N, Terauchi Y, Yamauchi T, Kubota T, Moroi M, Matsui J, Eto K, Yamashita T, Kamon J, Satoh H, Yano W, Froguel P, Nagai R, Kimura S, Kadowaki T, Noda T. 2002. Disruption of adiponectin causes insulin resistance and neointimal formation. J Biol Chem 277:25863–25866.

Lenchik L, Register TC, Hsu FC, Lohman K, Nicklas BJ, Freedman BI, Langefeld CD, Carr JJ, Bowden DW. 2003. Adiponectin as a novel determinant of bone mineral density and visceral fat. Bone 33:646–651.

Luo XH, Guo LJ, Yuan LQ, Xie H, Zhou HD, Wu XP, Liao EY. 2005. Adiponectin stimulates human osteoblasts proliferation and differentiation via the MAPK signaling pathway. Exp Cell Res 309:99–109.

Maeda K, Okubo K, Shimomura I, Funahashi T, Matsuzawa Y, Matsubara K. 1996. cDNA cloning and expression of a novel adipose specific collagen-like factor, apM1 (AdiPose Most abundant Gene transcript 1). Biochem Biophys Res Commun 221:286–289.

Matsubara M, Maruoka S, Katayose S. 2002. Inverse relationship between plasma adiponectin and leptin concentrations in normal-weight and obese women. Eur J Endocrinol 147:173–180.

Matsuzawa Y, Funahashi T, Kihara S, Shimomura I. 2004. Adiponectin and metabolic syndrome. Arterioscler Thromb Vasc Biol 24:29–33.

Nakano Y, Tobe T, Choi-Miura NH, Mazda T, Tomita M. 1996. Isolation and characterization of GBP28, a novel gelatin-binding protein purified from human plasma. J Biochem (Tokyo) 120:803–812.

Oshima K, Nampei A, Matsuda M, Iwaki M, Fukuhara A, Hashimoto J, Yoshikawa H, Shimomura I. 2005. Adiponectin increases bone mass by suppressing osteoclast and activating osteoblast. Biochem Biophys Res Commun 331:520–526.

Ouchi N, Kihara S, Arita Y, Okamoto Y, Maeda K, Kuriyama H, Hotta K, Nishida M, Takahashi M, Muraguchi M, Ohmoto Y, Nakamura T, Yamashita S, Funahashi T, Matsuzawa Y. 2000. Adiponectin, an adipocyte-derived plasma protein, inhibits endothelial NF-kappaB signaling through a cAMP-dependent pathway. Circulation 102:1296–1301.

Parfitt AM, Drezner MK, Glorieux FH, Kanis JA, Malluche H, Meunier PJ, Ott SM, Recker RR. 1987. Bone histomorphometry: Standardization of nomenclature, symbols, and units. Report of the ASBMR Histomorphometry Nomenclature Committee. J Bone Miner Res 2: 595–610.

Scherer PE, Williams S, Fogliano M, Baldini G, Lodish HF. 1995. A novel serum protein similar to C1q, produced exclusively in adipocytes. J Biol Chem 270:26746–26749.

Takeda S, Elefteriou F, Levasseur R, Liu X, Zhao L, Parker KL, Armstrong D, Ducy P, Karsenty G. 2002. Leptin regulates bone formation via the sympathetic nervous system. Cell 111:305–317.

Tanko LB, Christiansen C. 2004. Can confounding with fat-derived endogenous free estradiol explain the inverse correlation of bone mineral density with adiponectin? Bone 34:916; author reply 917.

Thomas DM, Hards DK, Rogers SD, Ng KW, Best JD. 1996. Insulin receptor expression in bone. J Bone Miner Res 11:1312–1320.

Thomas T, Gori F, Khosla S, Jensen MD, Burguera B, Riggs BL. 1999. Leptin acts on human marrow stromal cells to enhance differentiation to osteoblasts and to inhibit differentiation to adipocytes. Endocrinology 140:1630–1638.

Tremollieres FA, Pouilles JM, Ribot C. 1993. Vertebral postmenopausal bone loss is reduced in overweight women: A longitudinal study in 155 early postmenopausal women. J Clin Endocrinol Metab 77:683–686.

Tsao TS, Murrey HE, Hug C, Lee DH, Lodish HF. 2002. Oligomerization state-dependent activation of NF-kappa B signaling pathway by adipocyte complement-related protein of 30 kDa (Acrp30). J Biol Chem 277:29359–29362.

Ukkola O, Santaniemi M. 2002. Adiponectin: A link between excess adiposity and associated comorbidities? J Mol Med 80:696–702.

Weyer C, Funahashi T, Tanaka S, Hotta K, Matsuzawa Y, Pratley RE, Tataranni PA. 2001. Hypoadiponectinemia in obesity and type 2 diabetes: Close association with insulin resistance and hyperinsulinemia. J Clin Endocrinol Metab 86:1930–1935.

Yamauchi T, Kamon J, Waki H, Terauchi Y, Kubota N, Hara K, Mori Y, Ide T, Murakami K, Tsuboyama-Kasaoka N, Ezaki O, Akanuma Y, Gavrilova O, Vinson C, Reitman ML, Kagechika H, Shudo K, Yoda M, Nakano Y, Tobe K, Nagai R, Kimura S, Tomita M, Froguel P, Kadowaki T. 2001. The fat-derived hormone adiponectin reverses insulin resistance associated with both lipoatrophy and obesity. Nat Med 7:941–946.

Yamauchi T, Kamon J, Ito Y, Tsuchida A, Yokomizo T, Kita S, Sugiyama T, Miyagishi M, Hara K, Tsunoda M, Murakami K, Ohteki T, Uchida S, Takekawa S, Waki H, Tsuno NH, Shibata Y, Terauchi Y, Froguel P, Tobe K, Koyasu S, Taira K, Kitamura T, Shimizu T, Nagai R, Kadowaki T. 2003a. Cloning of adiponectin receptors that mediate antidiabetic metabolic effects. Nature 423:762–769.

Yamauchi T, Kamon J, Waki H, Imai Y, Shimozawa N, Hioki K, Uchida S, Ito Y, Takakuwa K, Matsui J, Takata M, Eto K, Terauchi Y, Komeda K, Tsunoda M, Murakami K, Ohnishi Y, Naitoh T, Yamamura K, Ueyama Y, Froguel P, Kimura S, Nagai R, Kadowaki T. 2003b. Globular adiponectin protected ob/ob mice from diabetes and ApoE-deficient mice from atherosclerosis. J Biol Chem 278:2461–2468.

Yokota T, Oritani K, Takahashi I, Ishikawa J, Matsuyama A, Ouchi N, Kihara S, Funahashi T, Tenner AJ, Tomiyama Y, Matsuzawa Y. 2000. Adiponectin, a new member of the family of soluble defense collagens, negatively regulates the growth of myelomonocytic progenitors and the functions of macrophages. Blood 96:1723–1732.

Yokota T, Meka CS, Medina KL, Igarashi H, Comp PC, Takahashi M, Nishida M, Oritani K, Miyagawa J, Funahashi T, Tomiyama Y, Matsuzawa Y, Kincade PW. 2002. Paracrine regulation of fat cell formation in bone marrow cultures via adiponectin and prostaglandins. J Clin Invest 109:1303–1310.

Yokota T, Meka CS, Kouro T, Medina KL, Igarashi H, Takahashi M, Oritani K, Funahashi T, Tomiyama Y, Matsuzawa Y, Kincade PW. 2003. Adiponectin, a fat cell product, influences the earliest lymphocyte precursors in bone marrow cultures by activation of the cyclooxygenase-prostaglandin pathway in stromal cells. J Immunol 171:5091–5099.

pH-Responsive Three-Layered PEGylated Polyplex Micelle Based on a Lactosylated ABC Triblock Copolymer as a Targetable and Endosome-Disruptive Nonviral Gene Vector

Motoi Oishi,[†] Kazunori Kataoka,*[,‡,#] and Yukio Nagasaki*[,†]

Tsukuba Research Center for Interdisciplinary Materials Science (TIMS), University of Tsukuba, 1-1-1 Ten-noudai, Tsukuba, Ibaraki 305-8573, Japan, Department of Materials Engineering, Graduate School of Engineering, The University of Tokyo, 7-3-1 Hongo, Bunkyo-ku, Tokyo 113-8656, Japan, and Division of Clinical Biotechnology, Center for Disease Biology and Integrative Medicine, Graduate School of Medicine, The University of Tokyo, 7-3-1 Hongo, Bunkyo-ku, Tokyo 113-0033, Japan. Received December 24, 2005; Revised Manuscript Received February 21, 2006

Nonviral vectors for gene therapy have recently received an increased impetus because of the inherent safety problems of the viral vectors, while their transfection efficiency is generally low compared to the viral vectors. The lack of the ability to escape from the endosomal compartments is believed to be one of the critical barriers to the intracellular delivery of noviral gene vectors. This study was devoted to the design and preparation of a novel ABC triblock copolymer for constructing a pH-responsive and targetable nonviral gene vector. The copolymer, lactosylated poly(ethylene glycol)-*block*-poly(silamine)-*block*-poly[2-(*N,N*-dimethylamino)ethyl methacrylate] (Lac-PEG-PSAO-PAMA), consists of lactosylated poly(ethylene glycol) (A-segment), a pH-responsive polyamine segment (B-segment), and a DNA-condensing polyamine segment (C-segment). The Lac-PEG-PSAO-PAMA spontaneously associated with plasmid DNA (pDNA) to form three-layered polyplex micelles with a PAMA/pDNA polyion complex (PIC) core, an uncomplexed PSAO inner shell, and a lactosylated PEG outer shell, as confirmed by ^{1}H NMR spectroscopy. Under physiological conditions, the Lac-PEG-PSAO-PAMA/pDNA polyplex micelles prepared at an N/P (number of amino groups in the copolymer/number of phosphate groups in pDNA) ratio above 3 were found to be able to condense pDNA, thus adopting a relatively small size (< 150 nm) and an almost neutral surface charge ($\zeta \sim +5$ mV). The micelle underwent a pH-induced size variation (pH = 7.4, 132.6 nm → pH = 4.0, 181.8 nm) presumably due to the conformational changes (globule-rod transition) of the uncomplexed PSAO chain in response to pH, leading to swelling of the free PSAO inner shell at lowered pH while retaining the condensed pDNA in the PAMA/pDNA PIC core. Furthermore, the micelles exhibited a specific cellular uptake into HuH-7 cells (hepatocytes) through asialoglycoprotein (ASGP) receptor-mediated endocytosis and achieved a far more efficient transfection ability of a reporter gene compared to the Lac-PEG-PSAO/pDNA and Lac-PEG-PAMA/pDNA polyplex micelles composed of the diblock copolymers and pDNA. The effect of hydroxychloroquine as an endosomolytic agent on the transfection efficiency was not observed for the Lac-PEG-PSAO-PAMA/pDNA polyplex micelles, whereas the nigericin treatment of the cell as an inhibitor for the endosomal acidification induced a substantial decrease in the transfection efficiency, suggesting that the protonation of the free PSAO inner shell in response to a pH decrease in the endosome might lead to the disruption of the endosome through buffering of the endosomal cavity. Therefore, the polyplex micelle composed of ABC (ligand-PEG/pH-responsive segment/DNA-condensing segment) triblock copolymer would be a promising approach to a targetable and endosome disruptive nonviral gene vector.

INTRODUCTION

Nonviral vectors for gene therapy have recently received increased attention because of the concerns over the safety issues of viral vectors, including immunogenicity, oncogenicity, and potential virus recombination (*1*−*3*). Most of the nonviral vectors developed so far, however, show low transfection efficiency compared to the viral vectors, because the latter have evolved multi-functionality to overcome the critical barrier to efficient gene delivery by directing the specific cellular uptake and enhancing transport to the cytoplasm from the endosomal compartment. Recently, a new class of nonviral gene vectors has been developed based on the supramolecular assembly between plasmid DNA (pDNA) and poly(ethylene glycol) (PEG)-*block*-polyamine copolymers (polyplex micelles) (*4*−*10*). Because of the highly dense PEG shell surrounding the polyion complex (PIC) core, the polyplex micelles exhibited excellent solubility in aqueous media, high tolerability toward nuclease degradation, and minimal interaction with biological components, including proteins and cells, compared to the other conventional polyplex and lipoplex systems. Furthermore, ligand-installed polyplex micelles prepared from lactosylated PEG-*block*-poly[2-(*N,N*-dimethylamino)ethyl methacrylate] copolymer and pDNA showed an increase in the cellular uptake through a receptor-mediated endocytosis process compared to those without lactose (ligand) moieties (*11*). To observe an appreciable effect of the ligand molecules on gene expression, however, the presence of hydroxychloroquine (100 μM) as an endosomolytic agent (*12*, *13*) has so far been required. This indicates that endosomal escape should be the most critical

* To whom correspondence should be addressed. (Y.N.) Phone: +81-29-853-5749. Fax: +81-29-853-5749. E-mail: nagasaki@nagalabo.jp; (K.K.) Phone +81-3-5841-7139. Fax: +81-3-5841-7139. E-mail: kataoka@bmw.t.u-tokyo.ac.jp.

[†] Tsukuba Research Center for Interdisciplinary Materials Science (TIMS), University of Tsukuba.

[‡] Department of Materials Engineering, The University of Tokyo.

[#] Division of Clinical Biotechnology, The University of Tokyo.

10.1021/bc050364m CCC: $33.50
Published on Web 04/15/2006

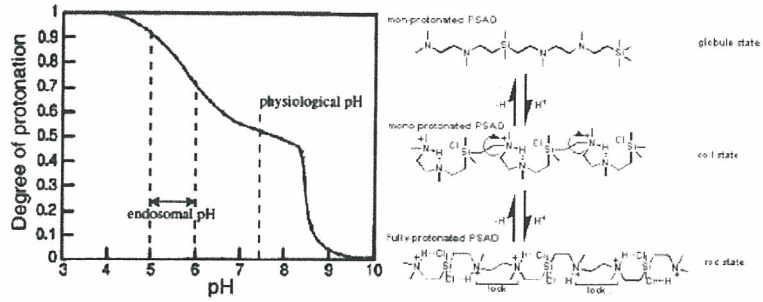

Figure 1. Change in the protonation degree of poly(silamine) (PSAO) with pH accompanying the conformation transition (globule-coil-rod).

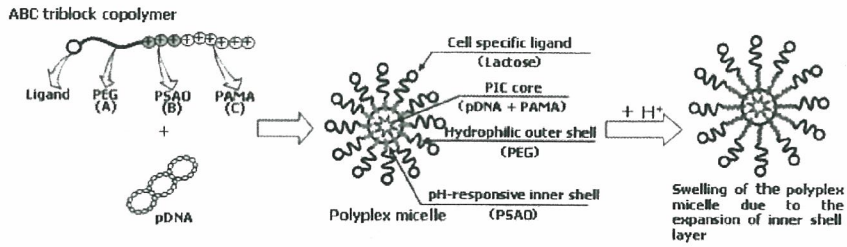

Figure 2. Schematic illustration of the formation of the three-layered polyplex micelle composed of the ABC triblock copolymer and pDNA.

barrier to intracellular gene delivery by polyplex micelles (*14*−*16*). Therefore, approaches are needed to devise polyplex micelles with a function to escape from the endosome where the pH is 1.4−2.4 units lower than the physiological pH of 7.4 (*17*−*20*). In this regard, poly(ethylenimine) (PEI) derivatives are of interest as a pH-responsive polyamine component to accomplish endosomal escape by taking advantage of their substantially lowered value of apparent pK_a (~5.5) ("buffer or proton-sponge effect") (*21*). However, the buffer effect of the PEI segment occurs only when an excess of amino groups with respect to DNA phosphate groups (high N/P ratio) is present in the system, where a considerable amount of the amino groups in PEI is in the free-base form. This fact strongly suggests that free PEI, which is not complexed with pDNA, is likely to play a crucial role in the buffer effect, because amino groups in the PEI/pDNA polyplex generally undergo facilitated protonation due to the zipper effect or the neighboring group effect during the polyion complexation (over-protonation) to decrease the buffering capacity (*22*). Therefore, a strategy is needed to satisfy the prevention of overprotonation of the pH-responsive polyamine segment in the polyplex, as well as the achievement of efficient condensation of pDNA into the PIC core to exert efficient stability. Worth noting in this regard is a concomitant incorporation of the polyamine segment with a high pK_a and one with a low pK_a into a single PEG-based strand, as an ABC triblock copolymer (*23*). A polyamine segment with a high pK_a as the C block preferentially forms a polyion complex with phosphate groups in pDNA (DNA-condensation segment), whereas the pH-responsive polyamine segment (B block) with a comparatively low pK_a, located between the PEG segment (A block) and the pDNA-condensation segment (C block), is expected to retain a substantial fraction of unprotonated amino groups (free-base) even in the polyplex due to the low protonation ability. As a consequence, the polyion complexation between such an ABC triblock copolymer and pDNA may lead to the formation of a three-layered polyplex micelle possessing an unprotonated pH-responsive polyamine segment as an intermediate layer to function as a buffering moiety for facilitated endosomal escape.

We herein synthesized a novel ABC triblock copolymer composed of a targetable and biocompatible polymer segment, a pH-responsive polyamine segment, and a DNA-condensing polyamine segment to form a three-layered polyplex micelle: lactosylated PEG-*block*-poly(silamine) (PSAO) -*block*-poly[2-(*N,N*-dimethylamino)ethyl methacrylate] (PAMA) [Lac-PEG-PSAO-PAMA]. Here, PSAO was selected as the pH-responsive polyamine segment showing two-step protonation (Figure 1, pK_{a1} = 8.6 and pK_{a2} = 5.8) along with a unique conformational transition at the critical pH (*24*−*29*). The unprotonated PSAO is insoluble in water, assuming a globular conformation with high flexibility, whereas fully protonated PSAO is soluble in water, assuming a rodlike conformation with rigid and expanded polymer strands. Such a unique conformational transition (rod-globule transition) can be explained by the rotational hindrance around the polymer chain due to the protonation of the amino groups along with the counteranion binding to the Si atoms (Figure 1). On the other hand, PAMA (pK_a = 7.2) is known to condense pDNA to form a compact structure, the size of which is less than 200 nm under physiological conditions (*8*, *30*, *31*). This fact suggests that polyion complexation between the Lac-PEG-PSAO-PAMA and pDNA may form a targetable and endosome disruptive polyplex micelle with a well-defined three-layered structure (Figure 2).

EXPERIMENTAL SECTION

Materials. 2,2′-Azobisisobutyronitrile (AIBN), dicyclohexylcarbodiimide (DCC), *N*-hydroxysuccinimide (NHS), and nigericin (NR) were purchased from Wako and used without further purification. Asialofetuine (ASF) and hydroxychloroquine sulfate (HCQ) were purchased from Sigma and Acros Organics, respectively. Potassium naphthalene was used as a THF solution, whose concentration was determined by titration. Water was purified using a Milli-Q instrument (Millipore). 2-Propanol and diethyl ether (Et_2O) were used as received without further purification. Lysotraker Red DND-99 was purchased from Molecular Probes. Plasmid DNA (pDNA) encoding firefly luciferase (pGL3-Luc, Promega; 5256 bpa) was amplified using EndoFree Plasmid Maxi or Mega kits (QIAGEN). The DNA concentration was determined by reading the absorbance at 260 nm.

Polymer Analysis. ^{1}H NMR (400 MHz) spectra were obtained in $CDCl_3$, DMSO-d_6, or D_2O (pD = 7.4 and 4.0) with 0.15 M NaCl using a JEOL EX400 spectrometer. Chemical shifts were reported in ppm relative to $CDCl_3$ (δ7.26, ^{1}H), DMSO-d_6 (δ 2.50, ^{1}H), or D_2O buffer (δ 4.76, ^{1}H). Size exclusion chromatography (SEC) was performed using a TOSO

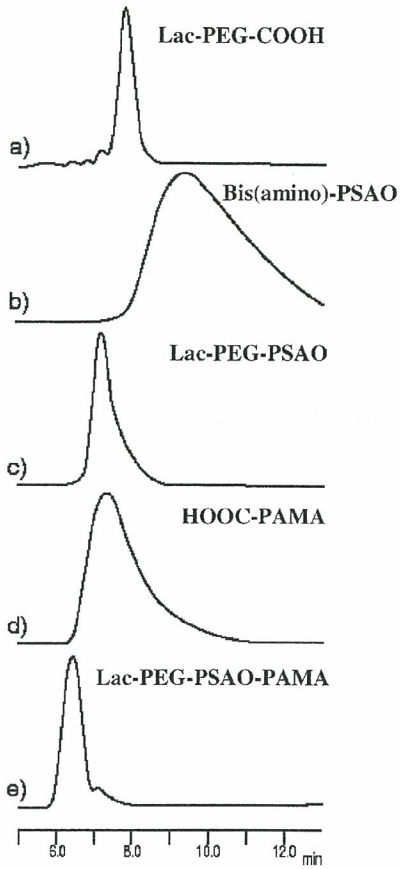

Figure 3. SEC chromatograms of the (a) Lac-PEG-COOH, (b) bis(amino)-PSAO, (c) Lac-PEG-PSAO block copolymer, (d) HOOC-PAMA, and (e) Lac-PEG-PSAO-PAMA triblock copolymer.

HLC-8020 equipped with an internal refractive index (RI) detector (RID-6A) with the combination of TSK G4000$_{HR}$ and G3000$_{HR}$ columns using THF as the eluent.

Synthesis of Lactose-PEG-*block*-PSAO. Bis(amino)-PSAO was synthesized according to our previous report (*24*−*29*). The Lac-PEG-COOH (0.100 g, 16 μmol) and an excess amount of bis(amino)-PSAO (1.244 g 800 μmol, M_n = 1550, DP = 6) were dissolved in $CHCl_3$ (5.0 mL) together with DCC (6.3 mg, 32 μmol) and NHS (2.3 mg, 20 μmol). The reaction mixture was stirred at room temperature for 72 h. To remove the unreacted bis(amino)-PSAO and other chemicals, the reaction mixture was poured into Et_2O (200 mL). The obtained polymer was further purified by reprecipitation into Et_2O (200 mL) and then freeze-dried with benzene to obtain the lactose-PEG-*b*-PSAO (0.102 g, 83% yield). Figures 3c and 4a, respectively, show the SEC chromatogram and ^{1}H NMR spectrum of Lac-PEG-PSAO with assignment. SEC M_n = 7170, M_w/M_n = 1.15 (calcd. M_n = 7850); ^{1}H NMR ($CDCl_3$, in Figure 4a) δ 0.10 (s, 36H, H_k), 0.63−0.79 (m, 24H, H_j), 1.02 (t, J = 7.3 Hz, 36H, H_i), 1.10 (t, J = 7.1 Hz, 3H, H_i''), 1.16 (t, J = 7.1 Hz, 3H, H_i'), 1.77−2.02 (m, 4H, H_d+H_f), 2.42 (t, J = 7.1 Hz, 2H, H_g), 2.47−2.62 (m, 80H, H_h), 2.62−2.73 (m, 2H, H_c), 3.61 (s, 617H, H_a+H_b+H_e)

Synthesis of Lactose-PEG-*block*-PSAO-*block*-PAMA. A PAMA homopolymer bearing a carboxylic acid group at the α-end (HOOC-PAMA) was synthesized via anionic polymerization of 2-(*N,N*-dimethylamino)ethyl methacrylate (*32*) using the allyl alcohol/potassium-naphthalene initiator system, followed by the radical addition of 3-mercaptopropionic acid in the presence of AIBN. The Lac-PEG-PSAO (0.051 g, 7.8 μmol) and an excess amount of HOOC-PAMA bearing a carboxylic acid group at the α-end (0.5017 g, 88.5 μmol, M_n = 5670, DP = 35) were dissolved in $CHCl_3$ (5.0 mL) together with DCC (3.2 mg, 16 μmol) and NHS (1.6 mg, 10 μmol). The reaction mixture was stirred at room temperature for 72 h. To remove the unreacted HOOC-PAMA and other chemicals, the polymer was recovered by precipitation into cold 2-propanol (−15 °C, 200 mL) and centrifuged for 45 min at 6000 rpm. Further purification was carried out by dialyzing against distilled, deionized water (cutoff MW 3500) and then freeze-dried to obtain Lac-PEG-PSAO-PAMA (0.0383 g, 37% yield). Figures 3e and 4b, respectively, show the SEC chromatogram and ^{1}H NMR spectrum of Lac-PEG-PSAO-PAMA with assignment. SEC M_n = 10850, M_w/M_n = 1.29 (calcd. M_n = 13450); ^{1}H NMR ($CDCl_3$, in Figure 4b) δ 0.10 (s, 36H, H_d), 0.63−0.79 (m, 24H, H_c), 0.80−1.16 (m, 94H, H_g), 1.02 (t, J = 7.3 Hz, 42H, H_e), 1.16−2.17 (m, 64H, H_f), 2.23 (s, 185H, H_j), 2.37−2.84 (m, 143H, H_b + H_i), 3.61 (s, 617H, H_a), 4.08 (s, 62H, H_h).

Light Scattering Measurements of Polyplex Micelles. To prepare stock solutions, specific amounts of each of the block copolymers (Lac-PEG-PSAO-PAMA, Lac-PEG-PSAO, and Lac-PEG-PAMA) were dissolved in 10 mM Tris-HCl buffer (pH 7.4) or distilled, deionized water, followed by adjustment of the pH to 7.4. Both solutions were filtered through a 0.1-μm filter to remove dust prior to the measurement. For the dynamic light scattering (DLS) measurements as a function of pH, the Lac-PEG-PSAO-PAMA copolymer in distilled water at pH 7.4 including 0.15 M NaCl was mixed with pDNA at an N/P ratio of 3 [N/P = (amino group in the block copolymer)/(phosphate groups in pDNA)] at pH 7.4 to obtain the final concentration of 33.3 μg/mL of pDNA in the solution. The sample solutions were adjusted to the desired pH using small aliquots of 0.1 or 0.01 M HCl, and the DLS was measured at each pH point (pH = 7.0, 6.5, 6.0, 5.5, 5.0, 4.5, and 4.0).

For the DLS measurements of the samples prepared at various N/P ratios, the block copolymer in 10 mM Tris-HCl buffer (pH 7.4) was mixed with pDNA at various N/P ratios (N/P = 1, 2, 3, 4, 5, 7, and 10), followed by the addition of 10 mM Tris-HCl buffer (pH 7.4) including 0.3 M NaCl to adjust the pDNA concentration (33.3 μg/mL) and the ionic strength of the solution to physiological conditions (0.15 M NaCl).

A light-scattering spectrometer (DLS-7000, Photal, Otsuka Electronics) equipped with a 75 mW Ar-laser that produces a vertically polarized incident beam at λ_0 = 488 nm was used in the present study for the DLS measurements.

During the DLS measurements, the autocorrelation function was analyzed using the cumulant method in which

$$g^{(1)}(\tau) = \exp[-\bar{\Gamma}\tau + (\mu_2/2)\tau^2 - (\mu_3/3!)\tau^3 + \cdots] \quad (1)$$

yielding an average characteristic line width of $\bar{\Gamma}$. The z-averaged diffusion coefficient was obtained from the $\bar{\Gamma}$ based on the following equations:

$$\bar{\Gamma} = Dq^2 \quad (2)$$

$$q = (4\pi n/\lambda)\sin(\theta/2) \quad (3)$$

where q is the magnitude of the scattering vector, n is the refractive index of the solvent, and θ is the detection angle. The hydrodynamic radius, d, can then be calculated using the Stokes−Einstein equation:

$$d = k_B T/(6\pi\eta D) \quad (4)$$

where k_B is the Boltzmann constant, T is the absolute temperature, and η is the viscosity of the solvent. Also, the polydispersity index (PDI = μ_2/Γ^2) was derived from eq 1.

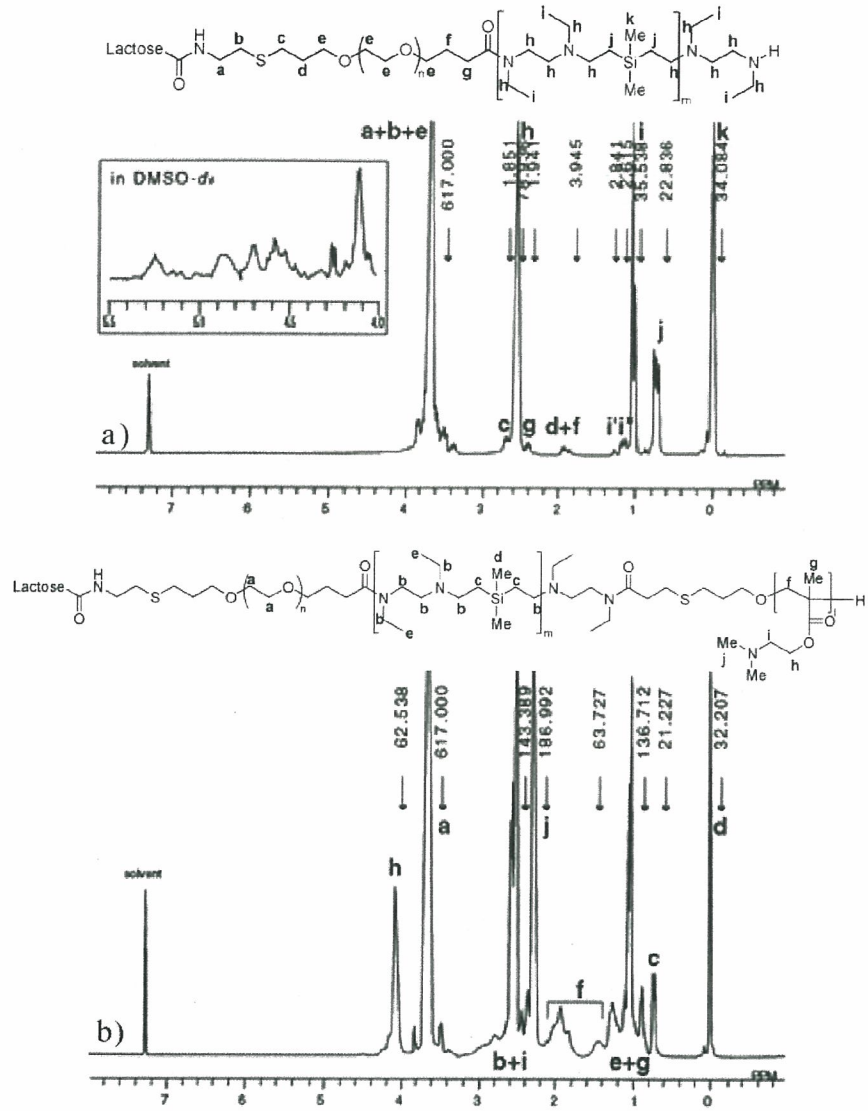

Figure 4. ^{1}H NMR spectra of (a) Lac-PEG-PSAO diblock copolymer and (b) Lac-PEG-PSAO-PAMA triblock copolymer.

Zeta-Potential Measurements. Laser-Doppler electrophoresis measurements of the polyplex micelles were carried out in 10 mM Tris-HCl buffer (pH 7.4) without NaCl (ELS-600, Photal, Otsuka Electronics). From the determined electrophoretic mobility, the zeta-potential (ζ) was calculated according to the Smoluchouski equation as follows:

$$\zeta = 4\pi n\eta\mu u/\epsilon \qquad (5)$$

where η is the viscosity of the solution, u is the electrophoretic mobility, and ϵ is the dielectric constant of the solvent.

Ethidium Bromide Exclusion Assay. The polyplex micelle solutions at various N/P ratios were mixed with ethidium bromide (EtBr) solution, and the final concentration was adjusted to [pDNA] = 20 μg/mL and [EtBr] = 0.4 μg/mL. The fluorescence of the intercalated EtBr was measured on a spectrofluorometer (F-2500, Hitachi) by exciting at 510 nm while monitoring emission at 590 nm.

Agarose Gel Retardation Studies. Aliquots (10 μL) of the above polyplex micelle solutions with various N/P ratios were mixed with 13 μL of running buffer of 3.3 mM Tris-AcOH with 1.0 mM EDTA2Na (pH 7.4) and loaded onto a 0.9 wt % agarose gel (50 V, 2 h). The amount of pDNA was adjusted to 0.3 μg of pDNA/lane. After EtBr (0.5 μg/mL) staining for 1 h, retardation of pDNA was visualized under UV irradiation.

Cell Culture. HuH-7 human cancer cells, derived from a hepatocarcinoma cell line, were obtained from the Cell Resource Center for Biomedical Research, Institute of Development, Aging and Cancer, Tohoku University. The cells were grown in Dulbecco's modified Eagle's medium (DMEM) supplemented with 10% FBS, 100 units/mL penicillin, and 100 μg/mL streptomycin at 37 °C in a humidified 5% CO_2 atmosphere.

Fluorescent Microscopy. Fluorescein isothiocyanate (FITC)-labeled pDNA was prepared using a Label IT nucleic acid labeling kit (Panvera). HuH-7 cells were seeded at a density of 5×10^5 cells/dish in a 35-mm glass bottom dish (Iwaki, Japan) and kept overnight at 37 °C in 5% CO_2 atmosphere. The Lac-PEG-PSAO-PAMA/pDNA polyplex micelles (N/P = 3) were added at a pDNA concentration of 30 μg/mL and incubated at 37 °C in 5% CO_2 atmosphere in the presence or absence of ASF (10 mg/mL) for 60 min. The cells were washed with phosphate buffered saline (PBS) three times and imaged directly in the cell culture medium using an Olympus IX70 with an appropriate filter.

Confocal Fluorescent Microscopy. HuH-7 cells were seeded at a density of 5×10^5 cells/dish in a 35-mm glass bottom dish

Scheme 1. Synthetic Route of Lac-PEG-PSAO-PAMA Block Copolymer

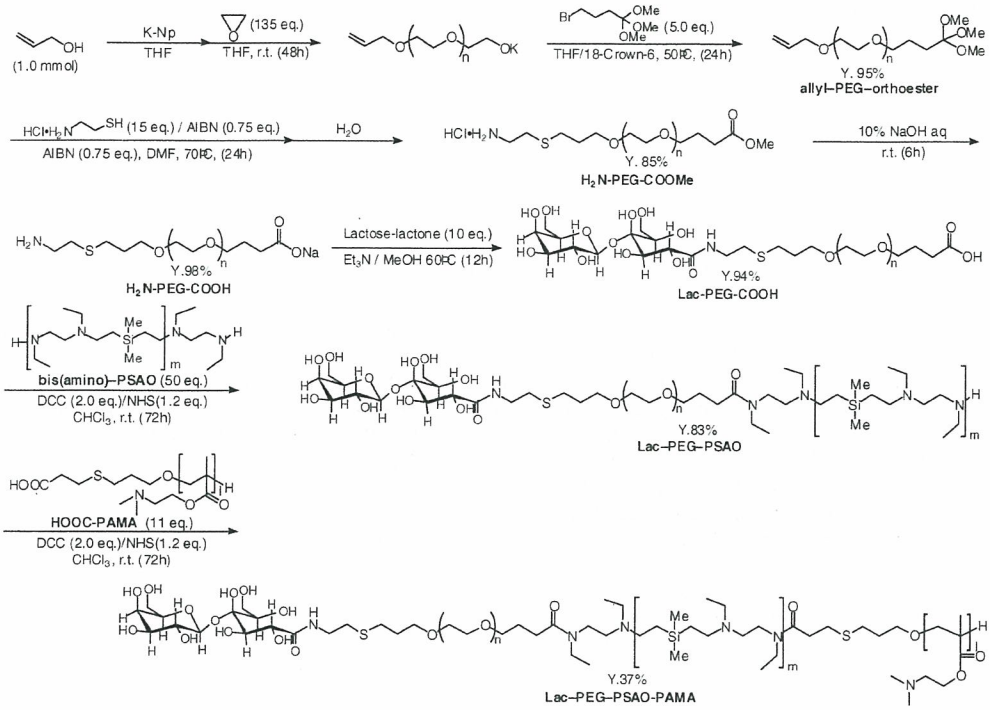

(Iwaki, Japan) and kept overnight at 37 °C in 5% CO_2 atmosphere. The Lac-PEG-PSAO-PAMA/pDNA and the Lac-PEG-PAMA/pDNA polyplex micelles (N/P = 3) containing FITC-labeled pDNA were added at a pDNA concentration of 30 μg/mL and incubated at 37 °C in 5% CO_2 atmosphere in the presence of Lysotraker Red DND-99 (50 nM) for 30 and 120 min. The cells were washed with PBS three times and imaged directly in the cell culture medium using an Olympus IX81 equipped with a confocal IX2-DSU system and an appropriate filter.

Transfection to HuH-7 Cells. HuH-7 cells were plated in a 24-well plate (5×10^4 cells/well) to reach about 50% confluence after 24 h at transfection, and the medium was then changed to fresh DMEM with 10% FBS (225 μL/well). For each well, the polyplex micelles or B-PEI/pDNA polyplexes at various N/P ratios (25 μL/well) were added with a pDNA concentration of 30 μg/mL. After 24 h incubation, the transfection medium was changed to fresh DMEM with 10% FBS, and the cells were further incubated for 24 h. For the preincubation study with serum, a medium containing 20% FBS was added to the solution of the polyplex micelles or B-PEI/pDNA polyplexes and incubated at 37 °C for 6 h prior to the transfection study. The cells were lysed, and the luciferase activity of the lysate was monitored with the a Luciferase Assay kit (Promega) and ARVOSX-1 (PerkinElmer). The results were expressed as light units per milligram of cell protein determined by a micro BCA assay kit (Pierce).

RESULTS AND DISCUSSION

Synthesis of Lactosylated Poly(ethylene glycol)-*block*-poly(silamine)-*block*-poly[2-(*N,N*-dimethlyamino)ethyl methacrylate] Triblock Copolymer. A synthetic route to lactosylated poly(ethylene glycol)-*block*-poly(silamine)-*block*-poy[2-(*N,N*-dimethlyamino)ethyl methacrylate] (Lac-PEG-PSAO-PAMA) triblock copolymer is shown in Scheme 1. A heterobifunctional PEG bearing an allyl group at the α-end and an ortho ester group at the ω-end (allyl-PEG-ortho ester) was synthesized via the anionic ring-opening polymerization of ethylene oxide using the allyl alcohol /potassium-naphthalene initiator system, followed by termination with trimethyl 4-bromoorthobutyrate in the presence of 18-Crown-6. The radical addition of 2-aminoethanethiol hydrochloride to the allyl-PEG-ortho ester quantitatively afforded an amine-PEG-methoxycarbonyl (H_2N-PEG-COOMe). Conversion of the ortho ester group into a methoxycarbonyl group (COOMe) occurred due to the hydrolysis of the ortho ester group during the purification (dialysis) process. The H_2N-PEG-COOMe was then converted into an amine-PEG-carboxylic acid (H_2N-PEG-COOH) by hydrolysis with 10% NaOHaq. The SEC (data not shown), ^{1}H NMR, and MALDI-TOF MS analyses (see Supporting Information) revealed that the determined molecular weight of the H_2N-PEG-COOH (SEC: M_n = 6200, M_w/M_n = 1.04, TOF-MS: M_n = 6190, M_w/M_n = 1.03) agrees well with the calculated value (calcd. M_n = 6130), and an amino group and carboxylic acid group were quantitatively introduced into the α-end and ω-end of PEG, respectively, to confirm the successful synthesis of allyl-PEG-ortho ester and H_2N-PEG-COOMe. The introduction of a lactose group to the amine end of H_2N-PEG-COOH was performed by reaction with an excess amount of lactose-lactone (*33*). In the ^{1}H NMR spectrum of Lac-PEG-COOH, the degree of lactose functionality was determined to be 72% (see Supporting Information).

To obtain the lactosylated PEG-PSAO block copolymer, bis(amino)-PSAO (M_n = 1550, the degree of polymerization (DP) = 6) was prepared as reported previously by the anionic polyaddition of dimethyldivinylsilane with *N,N'*-diethylethylenediamine in the presence of a catalytic amount of *n*-BuLi in THF at 60 °C (*24*−*29*). The conjugation of the Lac-PEG-COOH with bis(amino)-PSAO was performed by activating the terminal carboxylic acid of Lac-PEG-COOH using dicyclohexylcarbodiimide (DCC) and *N*-hydroxysuccinimide (NHS). A large excess (50 equiv) of the bis(amino)-PSAO was used to suppress the formation of triblock coplymer viz., Lac-PEG-PSAO-PEG-Lac. After the conjugation reaction, unconjugated bis(amino)-PSAO and other chemicals were removed by precipitation into Et_2O. Figures 3c and 4a, respectively, show the SEC chromatogram and ^{1}H NMR spectrum of the Lac-PEG-PSAO block

Table 1. Diameter (d), PDI (μ_2/Γ^2), and Zeta-Potential (ζ) of the Lac-PEG-PSAO-PAMA/pDNA, Lac-PEG-PAMA/pDNA, and Lac-PEG-PSAO/pDNA Polyplex Micelles Prepared at Various N/P Ratios

	Lac-PEG-PSAO−PAM A polyplex micelles		Lac-PEG-PAMA polyplex micelles		Lac-PEG-PSAO polyplex micelles	
N/P ratio	DLS[a] d (nm) /PDI (μ_2/Γ^2)	zeta-potential[b] (mV)	DLS[a] d (nm)/ PDI (μ_2/Γ^2)	zeta-potential[b] (mV)	DLS[a] d (nm)/ PDI (μ_2/Γ^2)	zeta-potential[b] (mV)
1	200.3/0.23	−4.3	196.5/0.24	−3.8	178.9/0.24	−5.8
2	175.4/0.23	+3.6	180.9/0.22	+3.8	166.6/0.20	−1.2
3	149.1/0.14	+4.7	147.0/0.14	+4.6	157.0/0.17	+0.6
4	147.2/0.17	+5.3	141.5/0.17	+4.8	163.4/0.22	+1.7
5	147.4/0.13	+5.1	140.0/0.19	+4.7	140.1/0.12	+2.3
7	146.8/0.18	+5.5	141.6/0.14	+5.0	144.7/0.19	+2.5
10	145.5/0.18	+5.4	136.1/0.12	+4.8	145.2/0.17	+2.4

[a] Conditions for DLS measurements: detection angle, 90°; solvent, 10 mM Tris-HCl, pH 7.4, including 0.15 M NaCl; temperature, 37 °C. [b] Conditions for zeta-potential measurements: solvent, 10 mM Tris-HCl, pH 7.4; temperature, 25 °C.

copolymer with assignments. As seen in the SEC chromatograms (Figure 3), Lac-PEG-PSAO (Figure 3c) gave a unimodal peak at a high molecular weight position (i.e., shorter elution time) compared to the Lac-PEG-COOH (M_n = 6300, M_w/M_n = 1.05, Figure 3a) and bis(amino)-PSAO (M_n = 1550, M_w/M_n = 2.01, Figure 3b). Note that the unreacted Lac-PEG-COOH and bis(amino)-PSAO were not observed in the SEC chromatogram (Figure 3c) of the Lac-PEG-PSAO (obsd. M_n = 7150, M_w/M_n = 1.15, calcd. M_n = 7850). In the ^{1}H NMR spectrum (Figure 4a), the peaks corresponding to both of the PEG and PSAO segments were clearly observed, consistent with the formation of a diblock copolymer. Note that the peaks corresponding to the terminal lactose moiety were also observed at δ 4.0−5.3 ppm in the ^{1}H NMR spectrum in DMSO-d_6. From the integral ratio between the PEG-backbone protons (3.7 ppm -OCH_2CH_2-) and the methyl protons of PSAO segment (0.1 ppm, $SiMe_2$), the DP of the PSAO segment in the block copolymer was calculated to be 5.67, which is in good accordance with that of the starting bis(amino)-PSAO (DP = 6).

To obtain the Lac-PEG-PSAO-PAMA triblock copolymer, the conjugation of the Lac-PEG-PSAO diblock copolymer and HOOC-PAMA was performed in a manner similar to the conjugation of Lac-PEG-COOH and bis(amino)-PSAO. After the conjugation reaction, unconjugated HOOC-PAMA and other chemicals were removed by precipitation into cold 2-propanol, followed by centrifugation. Figures 3e and 4b, respectively, show the SEC chromatogram and ^{1}H NMR spectrum of the Lac-PEG-PSAO-PAMA triblock copolymer with assignments. The Lac-PEG-PSAO-PAMA (Figure 3e, M_n = 10850, M_w/M_n = 1.29, calcd. M_n = 13450) had a shorter elution time compared to the Lac-PEG-PSAO (M_n = 7170, M_w/M_n = 1.15, Figure 3c) and HOOC-PAMA (M_n = 5670, M_w/M_n = 1.50, DP = 35, Figure 3d), indicating an increased molecular weight due to the formation of the triblock polymer. Nevertheless, a slight portion of unreacted Lac-PEG-PSAO and/or HOOC-PAMA seems to still remain (about 10%) in the sample as indicated by the small accompanying peak appearing after the main fraction (Figure 3e). In thethe ^{1}H NMR spectrum (Figure 4b), the peaks corresponding to the PEG, PSAO, and PAMA segments were clearly observed, suggesting the formation of a triblock copolymer. From the integral ratio between the PEG-backbone protons (3.7 ppm -OCH_2CH_2-) and methylene protons of the PAMA segment (4.08 ppm, -COOCH_2CH_2N(CH_3)$_2$), the DP of the PAMA segment was calculated to be 31.3 (DP of starting PAMA = 35). This result indicates that the purity of the triblock copolymer was 89%.

Furthermore, Lac-PEG-PSAO (M_{nPEG} = 6300, DP_{PSAO} = 6, number of amino groups = 12) and Lac-PEG-PAMA (M_{nPEG} = 6300, DP_{PAMA} = 55, number of amino groups = 55) diblock copolymers were prepared in a similar manner as the controls for the Lac-PEG-PSAO-PAMA (M_{nPEG} = 6300, DP_{PSAO} = 6, DP_{PAMA} = 35, total number of amino groups = 47).

Physicochemical Characterization of Polyplex Micelles. The obtained triblock (Lac-PEG-PSAO-PAMA) and diblock (Lac-PEG-PAMA and Lac-PEG-PSAO) copolymers form polyplex micelles through the mixing with pDNA based on electrostatic interaction. The size and surface charge of the polyplex micelles (Lac-PEG-PSAO-PAMA/pDNA, Lac-PEG-PAMA/pDNA, and Lac-PEG-PSAO/pDNA) was respectively evaluated by dynamic light scattering (DLS) and Laser-Doppler electrophoresis measurements at various N/P ratios, as summarized in Table 1. In the DLS measurements, the diameter (d) and polydipersity index (PDI; μ_2/Γ^2) of all the polyplex micelles decreased with increasing N/P ratios and reached plateau values of ca. 150 nm and 0.2, respectively, at an N/P ratio higher than 5. Concomitantly, as the N/P ratios increased, the zeta-potential (ζ) of all the polyplex micelles gradually shifted from a negative value ($\zeta < 0$) to a positive value ($\zeta > 0$). Nevertheless, the zeta-potential of all the polyplex micelles retained only a slightly positive value (ζ = +5 mV) even when the N/P ratio was increased to 10, suggesting the formation of a PEG corona surrounding the PIC core. These phenomena are consistent with the DNA condensation (coil-globule transition) upon complexation with the polycation segment in the block copolymers (*5*, *9*, *10*). It should also be noted that the N/P ratio to induce complete DNA condensation substantially shifted to a higher value from a stoichiometric mixing ratio (N/P = 1). A similar tendency was observed for the polyplex micelle from the PEG-PAMA block copolymer and pDNA (*4*).

To further clarify the behavior of DNA condensation, the quenching of the fluorescence intensity of the DNA intercalating dye, EtBr, was observed under physiological conditions for all of the polyplex micelles. Note that cationic EtBr is excluded from the DNA minor groove with the progress of the charge neutralization and the subsequent condensation of DNA due to the interaction with polycations, and therefore, this characteristic of EtBr is frequently utilized to estimate the degree of DNA condensation through complexation with a polycation. The profiles are shown in Figure 5a. In line with a trend in the hydrodynamic diameter and zeta-potential variations as shown in Table 1, the fluorescence intensity of EtBr decreased with increasing N/P ratios for all of the polyplex micelles, and the quenching of the fluorescence still continued even in the region of N/P > 1, suggesting that DNA condensation was not completely finished at the stoichiometric mixing ratio (N/P = 1) and that a nonstoichiometric complex may form in the range of N/P > 1. It should be noted that the amino groups of both PAMA and PSAO segments are incompletely protonated at physiological pH (= 7.4) because of their relatively lowered pKa values (PAMA: pK_a = 7.2, and PSAO: pK_{a1} = 8.6, pK_{a2} = 5.8). This may be a reason for the shift of the DNA-condensation point from a stoichiometric mixing ratio (N/P = 1). It should also be noted that a 35% decrease in fluorescence intensity compared to the initial value was observed for Lac-PEG-PSAO, whereas a decrease is more significant (50∼55%)

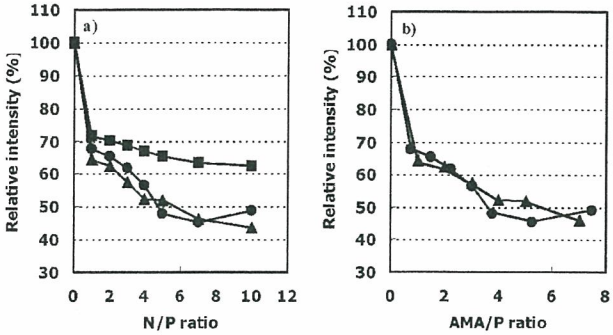

Figure 5. Ethidium bromide (EtBr) exclusion assay for the Lac-PEG-PSAO-PAMA/pDNA (circle), Lac-PEG-PAMA/pDNA (triangle), and Lac-PEG-PSAO/pDNA (square) systems. (a) Change in relative fluorescence intensity with the N/P ratio. (b) Change in relative fluorescence intensity with the AMA/P unit ratio ([amino groups in the PAMA segment]/[phosphate group in the pDNA]) (solvent, 10 mM Tris-HCl buffer including 0.15 M NaCl (pH 7.4); temperature, 37 °C).

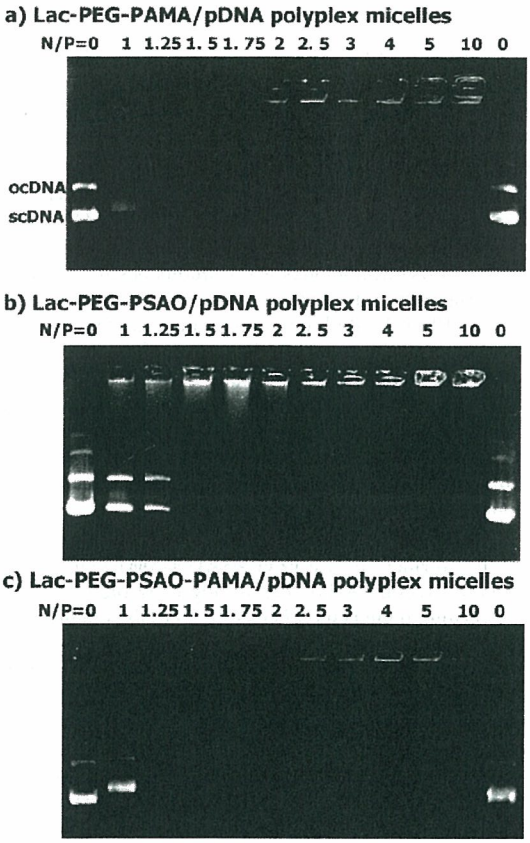

Figure 6. Agarose gel electrophoresis of the (a) Lac-PEG-PAMA/pDNA, (b) Lac-PEG-PSAO/pDNA, and (c) Lac-PEG-PSAO-PAMA/pDNA polyplex micelles prepared at various N/P ratios.

for Lac-PEG-PAMA and Lac-PEG-PSAO-PAMA, and their fluorescence intensities of Lac-PEG-PSAO-PAMA were almost identical when the N/P ratio was converted to the AMA/P ([amino groups in the PAMA segment]/[phosphate group in the pDNA]) unit ratio (Figure 5b), suggesting that the PAMA segment may preferentially take part in the complexation with DNA in the Lac-PEG-PSAO-PAMA/pDNA system, bearing the PSAO segment in the free form.

To evaluate the stability of the polyplex micelle, an agarose gel retardation assay at various N/P ratios was carried out. As shown in Figure 6, two topologically different forms of pDNA, i.e., supercoiled (scDNA) and open circular (ocDNA), were clearly observed in the absence of the block copolymer (at N/P = 0). In the cases of Lac-PEG-PSAO-PAMA/pDNA and Lac-PEG-PAMA/pDNA polyplex micelles, pDNA migration was completely retarded at an N/P ratio ≥ 1.5 (Figure 6a,c). Alternatively, a higher N/P ratio (≥ 3) was required for the complete retardation of pDNA for Lac-PEG-PSAO/pDNA polyplex micelles (Figure 6b). Presumably, excess cationic component may be needed for the Lac-PEG-PSAO block copolymer with a shorter cationic segment to induce effective DNA stabilization.

The polyplex micelle from Lac-PEG-PSAO-PAMA and pDNA was characterized by ^{1}H NMR spectroscopy in D_2O containing 0.15 M NaCl at pD = 7.4. Figure 7f shows the ^{1}H NMR spectrum of the polyplex micelle prepared at N/P = 3, where the residual molar ratio of the protonated PAMA segment in the block copolymer, calculated from the pK_a value, to the phosphate groups in pDNA is estimated to be unity at physiological pH (= 7.4). Note that the DNA condensation process was almost completed at N/P = 3, as shown in Table 1. Obviously, the peaks from the PAMA segment, which were clearly observed in the spectrum of the free polymers (Figure 7c), nearly disappeared upon complexation with pDNA (Figure 7f), whereas the peaks from the PSAO segment were still clearly observed in the spectrum. The selective disappearance of PAMA peaks upon complexation strongly suggests that the PAMA segment predominantly forms a PIC with pDNA to cause significant peak broadening. On the other hand, observation of the peaks from the PSAO segment even in the spectrum of the polyplex micelle suggests the presence of the uncomplexed PSAO fraction. Eventually, these results are consistent with the formation of the three-layered structure of the polyplex micelle with a PAMA/pDNA PIC core, a free PSAO inner shell, and a lactosylated PEG outer shell, as illustrated in Figure 2. In sharp contrast to the Lac-PEG PSAO-PAMA/pDNA system, peaks corresponding to polyamine segments (PAMA and PSAO) completely disappeared in the NMR spectra of the polyplex micelles from diblock copolymers (Lac-PEG-PAMA/pDNA (Figure 7d) and Lac-PEG-PSAO/pDNA (Figure 7e)) due to the limited molecular motion in the complex form.

pH Response of the Polyplex Micelles. To estimate the effect of the environmental pH on the hydrodynamic diameter of the polyplex micelles, the Lac-PEG-PSAO-PAMA/pDNA, Lac-PEG-PSAO/pDNA, and Lac-PEG-PAMA/pDNA polyplex micelles were prepared in 0.15 M NaClaq (pH 7.4) at N/P = 3. By decreasing the pH from 7.4 to 4.0, the diameter (d) of the Lac-PEG-PSAO-PAMA/pDNA and Lac-PEG-PSAO/pDNA polyplex micelles proportionally increases with a unimodal distribution ($\mu_2/\Gamma^2 < 0.25$), reaching a 2.7-times larger hydrodynamic volume at pH 4.0 compared to that at pH 7.4, as shown in Figure 8. On the contrary, there was negligible change in the hydrodynamic diameter of the Lac-PEG-PAMA/pDNA polyplex micelle with decreasing pH from 7.4 to 4.0. This pH-induced size variation observed for the system containing the PSAO segment is most likely to be related to the conformational changes in the PSAO chain due to progressive protonation with decreasing pH. In the ^{1}H NMR spectrum of the Lac-PEG-PAMA/pDNA polyplex micelle (N/P = 3) at pD = 4.0, the peaks from the PAMA segment almost disappeared, indicating that pDNA was still condensed even at pD = 4.0 by the PAMA segment (see Supporting Information). Furthermore, the ^{1}H NMR spectrum of the Lac-PEG-PSAO-PAMA/pDNA polyplex micelle at pD = 4.0 shows only the peaks assigned to the PSAO segment along with the PEG segment, suggesting the three-layered structure even at pD = 4.0 (see Supporting Information). This result supports the plausible scheme that the globule-to-rod conformational changes in the uncomplexed PSAO segment in the three-layered Lac-PEG-PSAO-PAMA/pDNA polyplex

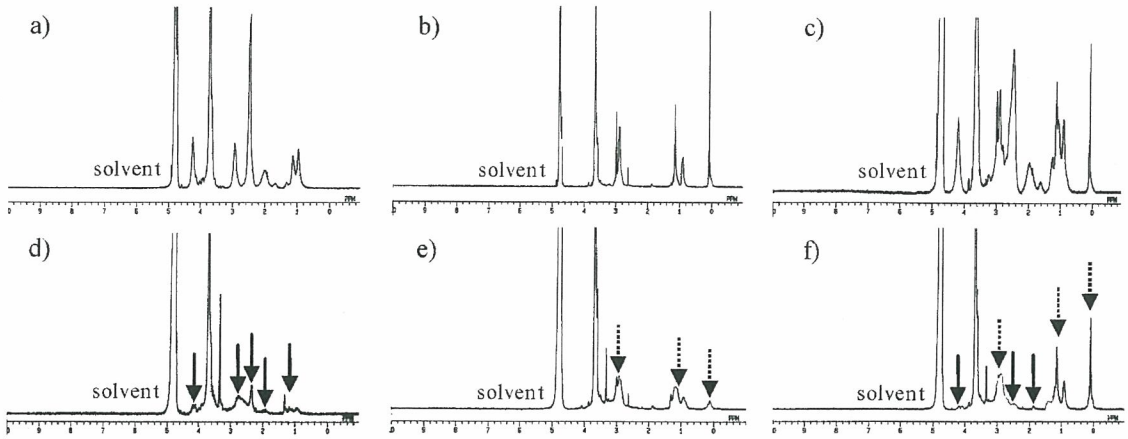

Figure 7. ^{1}H NMR spectra of (a) the Lac-PEG-PAMA block copolymer at pD = 7.4, (b) the Lac-PEG-PSAO block copolymer at pD = 7.4, (c) Lac-PEG-PSAO-PAMA triblock copolymer at pD = 7.4, (d) the Lac-PEG-PAMA/pDNA polyplex micelle at pD = 7.4, (e) the Lac-PEG-PSAO/pDNA polyplex micelle at pD = 7.4, and (f) the Lac-PEG-PSAO-PAMA/pDNA polyplex micelle at pD = 7.4 in D_2O containing 0.15 M NaCl at 37 °C. The solid and dotted arrows indicate the peaks corresponding to the PAMA segment and PSAO segment, respectively.

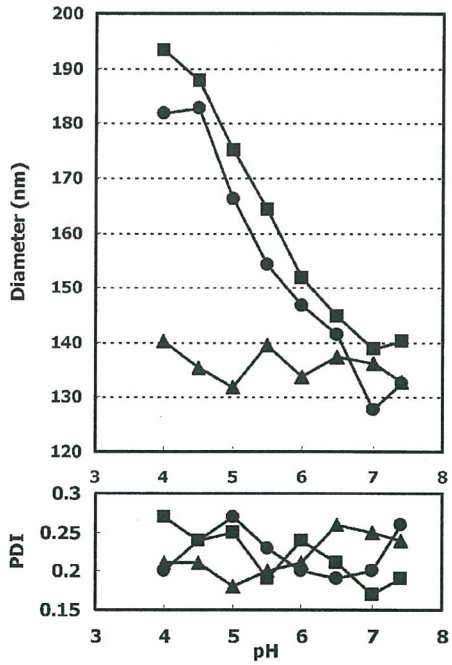

Figure 8. pH vs diameter (d) and PDI (μ_2/Γ^2) of the Lac-PEG-PSAO-PAMA/pDNA (circle), Lac-PEG-PAMA/pDNA (triangle), and Lac-PEG-PSAO/pDNA (square) polyplex micelles at N/P = 3 (angle, 90°; solvent, distilled water including 0.15 M NaCl; temperature, 37 °C).

micelle may induce the selective expansion of the PSAO inner shell while retaining the condensed pDNA in the PAMA/pDNA PIC core, leading to the remarkable pH-induced size variation. However, the observed size variation is clearly too large compared with the calculated PSAO length as the fully stretched chains for coil-state (pH 7.4) and rod-state (pH 4.0), indicating that the expansion of the PSAO inner shell is not sufficient to account for the size variation of the micelles. Although other possible factors probably exist, we believe that the expansion of the PSAO inner shell is one of the factor for the size variation of the micelles. On the other hand, the peaks from the PSAO segment clearly appeared in the ^{1}H NMR spectrum of the Lac-PEG-PSAO/pDNA polyplex micelle at pD = 4.0, suggesting that the conformational changes (globule-rod transition) of the complexed PSAO segment in the Lac-PEG-PSAO/pDNA polyplex micelle presumably leads to the formation of a loose PIC core (see Supporting Information). Apparently, the high rigidity of the protonated PSAO chain in the lower pH region should be unfavorable for triggering the DNA condensation upon complexation. As a consequence, a loose complex may form between pDNA and the PSAO segment without condensation in the lower pH region, showing an appreciable size increase.

Evaluation of the Biological Efficacy of the Polyplex Micelles. The cytotoxicity of the Lac-PEG-PSAO-PAMA, Lac-PEG-PAMA, and Lac-PEG-PSAO block copolymers against HuH-7 cells (hepatocytes) was studied using an MTT assay (see: Supporting Information). The viability of cells treated with the Lac-PEG-PSAO block copolymer was less than 20% at a polymer concentration of 100 μg/mL (IC_{50} < 30 μg/mL). In contrast, cells incubated with Lac-PEG-PSAO-PAMA or Lac-PEG-PAMA retained 65~70% viability relative to controls even at concentrations up to 100 μg/mL. This result indicates that the inclusion of PSAO segment into the Lac-PEG-PSAO-PAMA triblock copolymer seems to substantially reduce its inherent cytotoxicity.

To examine whether the lactose moiety (galactose terminal) on the surface of Lac-PEG-PSAO-PAMA/pDNA polyplex micelle is recognized by the asialoglycoprotein (ASGP) receptors existing on the HuH-7 cells (*34*, *35*), the cellular association and internalization of the polyplex micelle (N/P = 3) with fluorescein isothiocyanate (FITC)-labeled pDNA were visualized under a fluorescence microscope at 60 min of incubation in the presence and absence of asialofetuine (ASF). Note that the ASF is known to function as a competitive inhibitor for the ASGP receptor-mediated endocytosis (*36*). The cellular association and internalization of the Lac-PEG-PSAO-PAMA/pDNA polyplex micelle to HuH-7 cells in the absence of ASF were clearly observed as shown in Figure 9b,d. On the contrary, substantially reduced cellular association and internalization of the micelles were observed in the presence of ASF as shown in Figure 9a,c. This result indicates that the cellular association and internalization of the Lac-PEG-PSAO-PAMA/pDNA polyplex micelle occur mainly through the ASGP receptor-mediated process, which is inhibited in the presence of ASF (*37*).

To estimate the transfection ability of the Lac-PEG-PSAO-PAMA/pDNA, Lac-PEG-PAMA/pDNA, and Lac-PEG-PSAO/pDNA polyplex micelles with various N/P ratios, a transfection study using HuH-7 cells was carried out in the presence of 10% FBS. A pGL-3 control plasmid DNA encoding firefly luciferase was used as a reporter gene. In addition, the B-PEI/pDNA polyplex was used as a control vector at the optimal N/P ratio of 10 to show the highest transfection efficacy. As shown in Figure 10, the transfection efficiency of the Lac-PEG-PSAO-

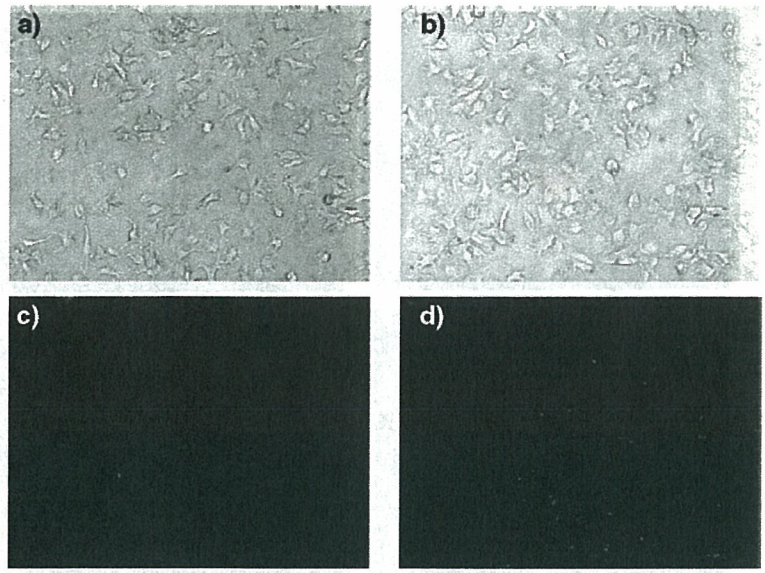

Figure 9. Association and internalization to HuH-7 cells of the Lac-PEG-PSAO-PAMA/pDNA polyplex micelles prepared at N/P = 3 after 60 min incubation. (a) ASF (+) (phase-contrast image), (b) ASF (−) (phase-contrast image), (c) ASF (+) (fluorescent image), and (d) ASF (−) (fluorescent image).

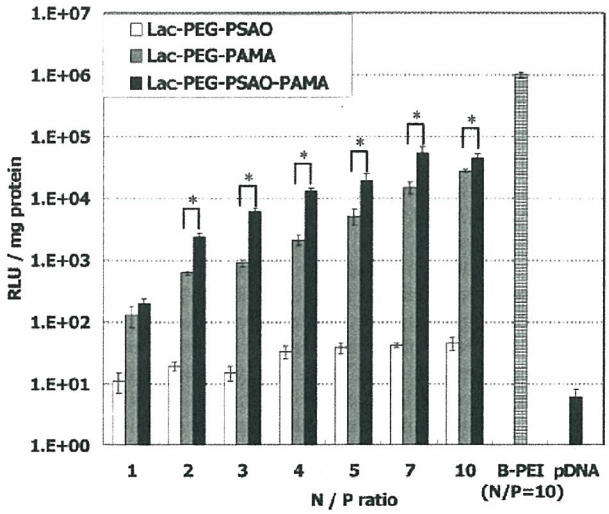

Figure 10. Transfection efficiency to HuH-7 cells of the Lac-PEG-PSAO-PAMA/pDNA, Lac-PEG-PAMA/pDNA, and Lac-PEG-PSAO/pDNA polyplex micelles prepared at various N/P ratios with a fixed pDNA amount. The plotted data are the average of triplicate experiments ± SD ($P^* < 0.05$).

PAMA/pDNA and Lac-PEG-PAMA/pDNA polyplex micelles was substantially improved with an increasing N/P ratio. In particular, 1 order of magnitude increase in transfection efficiency was achieved by increasing the N/P ratio from 1 to 2 ($P < 0.05$), corresponding to the formation of a stable polyplex structure judging from the agarose gel retardation assay, seen in Figure 6. Alternatively, the Lac-PEG-PSAO/pDNA polyplex micelles exhibited only limited transfection efficiency, presumably due to the low DNA condensing capacity of the PSAO chain as indicated from the results of the EtBr exclusion assay shown in Figure 5. Thus, polyplex micelles formed from Lac-PEG-PSAO may not be stable enough to be tolerated in the culture medium containing a substantial amount of serum proteins. Of interest, the transfection efficiency of the Lac-PEG-PSAO-PAMA/pDNA polyplex micelles always revealed a higher transfection efficiency than the Lac-PEG-PAMA/pDNA polyplex micelles in the range of N/P ratios between 2 and 10 ($P < 0.05$).

To determine whether the difference in the transfection efficiency between the Lac-PEG-PSAO-PAMA/pDNA and Lac-PEG-PAMA/pDNA polyplex micelles is related to the endosomal escape function, confocal microscope experiments were performed on the HuH-7 cells treated with the polyplex micelles containing FITC-labeled pDNA. Cells were co-incubated with LysoTracker Red DND-99 probe, which specifically stains acidic organelles such as endosomes and lysosomes. Thus, the colocalization of the polyplex micelles and the LysoTracker Red probe in an acidic compartment (endosome and lysosome) should be detected as yellow (or orange) fluorescence due to the merging of green and red colors. In the case of the Lac-PEG-PAMA/pDNA polyplex micelles (Figure 11a,b), the yellow and red fluorescences were observed without isolated green fluorescence even after a 120-min incubation, indicating that the polyplex micelles localized in the endosomes and/or lysosomes with the LysoTracker Red probe. The Lac-PEG-PSAO-PAMA/pDNA polyplex micelles localized in the endosomes and/or the lysosomes with the LysoTracker Red probe after a 30 min incubation (Figure 11c), as suggested by the partially yellow fluorescence. At 120 min of incubation, diffused green fluorescence was observed in the cytoplasm (Figure 11d), indicating that the Lac-PEG-PSAO-PAMA/pDNA polyplex micelles gradually escaped from the endosomes and/or lysomes into the cytoplasm in a time-dependent manner. These results suggest that both the PAMA segment as a DNA-condensing polycation and the PSAO segment as the buffering moiety may synergistically contribute to enhance the transfection efficiency of the Lac-PEG-PSAO-PAMA/pDNA polyplex micelles. Although the Lac-PEG-PSAO-PAMA/pDNA polyplex micelles showed 1 order of magnitude lower transfection efficiency than the B-PEI/pDNA polyplex at N/P = 10 ($P < 0.05$), this value may still be appreciable considering that the polyplexe micelles have hydrophilic and neutral PEG palisades on their surface to shield the cationic character.

To verify that the improved transfection ability of the Lac-PEG-PSAO-PAMA/pDNA polyplex micelles is a result of the facilitated endosomal escape function as well as the enhanced cellular uptake through ASGP-mediated endocytosis, the transfection study at N/P = 3, 5, and 10 was carried out in the presence or the absence of hydroxychloroquine (HCQ) as an endosomolytic agent, nigericin (NR) (*38*) as an inhibitor of the